

# Mo(VI) potential metallodrugs. Explaining the transport and cytotoxicity by chemical transformations

*Monalisa Mohanty,<sup>†</sup> Gurunath Sahu,<sup>†</sup> Atanu Banerjee,<sup>†</sup> Sudhir Lima,<sup>†</sup> Sushree Aradhana Patra,<sup>†</sup> Aurélien Crochet,<sup>‡</sup> Giuseppe Sciortino,<sup>§</sup> Daniele Sanna,<sup>§</sup> Valeria Ugone,<sup>§</sup> Eugenio Garribba,<sup>\*,||</sup> and Rupam Dinda<sup>\*,†</sup>*

<sup>†</sup>Department of Chemistry, National Institute of Technology, Rourkela 769008, Odisha, India.

<sup>‡</sup>Department of Chemistry, Fribourg Center for Nanomaterials, University of Fribourg, CH-1700 Fribourg, Switzerland.

<sup>§</sup>Institute of Chemical Research of Catalonia (ICIQ), The Barcelona Institute of Science and Technology (BIST), 43007 Tarragona, Spain.

<sup>§</sup>Istituto di Chimica Biomolecolare, Consiglio Nazionale delle Ricerche, Trav. La Crucca 3, I-07100 Sassari, Italy.

<sup>||</sup>Dipartimento di Scienze Mediche, Chirurgiche e Sperimentali, Università di Sassari, Viale San Pietro, I-07100 Sassari, Italy.

Corresponding authors. E-mail: garribba@uniss.it (E.G.); rupamdinda@nitrrkl.ac.in (R.D.).

## ABSTRACT

The transport and cytotoxicity of molybdenum-based drugs have been explained with the concept of chemical transformation, a very important idea in inorganic medicinal chemistry that is often overlooked in the interpretation of the biological activity of metal-containing systems. Two monomeric  $[\text{MoO}_2(\text{L}^1)(\text{MeOH})]$  (**1**)  $[\text{MoO}_2(\text{L}^2)(\text{EtOH})]$  (**2**) and two mixed-ligand dimeric  $[\{\text{MoO}_2(\text{L}^{1-2})\}_2(\mu\text{-4,4'-bipy})]$  (**3-4**)  $\text{Mo}^{\text{VI}}\text{O}_2$  species were synthesized and characterized. The structures of the solid complexes were solved through SC-XRD, while their transformation in water was clarified by UV-Vis, ESI-MS and DFT. In aqueous solution **1-4** lead to the penta-coordinated  $[\text{MoO}_2(\text{L}^{1-2})]$  active species after the release of the solvent molecule (**1-2**) or removal of the co-ligand 4,4'-bipy bridge (**3-4**).  $[\text{MoO}_2(\text{L}^{1-2})]$  are stable in solution and do not react with serum bioligand nor with cellular reductants. The binding affinity of **1-4** towards DNA and HSA were evaluated through analytical and computational methods and in both cases a non-covalent interaction is expected. Furthermore, the *in vitro* cytotoxicity of the complexes was also evaluated and flow cytometry analysis showed the apoptotic death of the cancer cells. Interestingly, the  $\mu\text{-4,4'-bipy}$  bridged complexes **3-4** were found to be more active than the monomeric **1-2**, due to the mixture of species generated that is  $[\text{MoO}_2(\text{L}^{1-2})]$  and the cytotoxic 4,4'-bipy after their dissociation. Since in the cytosol the reduction of  $\text{Mo}^{\text{VI}}$  to  $\text{Mo}^{\text{V/IV}}$  does not take place nor reactive oxygen species (ROS) are produced in Fenton-like reactions of **1-4** with  $\text{H}_2\text{O}_2$ , the mechanism of cytotoxicity should be attributable to the direct binding with DNA that occur with a minor-groove binding which results in the cell death through an apoptotic mechanism.

**Keywords:** Mo(VI) / Aroylhydrazones / Metallodrugs / Protein and DNA interaction / Cytotoxicity

## INTRODUCTION

Despite the rapid development of anticancer drugs, cancer remains one of the leading causes of death worldwide. This is due to the associated disadvantages of prevalent chemotherapeutic drugs like high toxicity to normal cells, limited ranges of activities, acquired tumour resistance, and metastasis (secondary) cancers.<sup>1,2</sup> Therefore, in an attempt to replace these drugs with suitable alternatives, numerous transition metal complexes are being synthesized and tested for their anticancer activities.

For the design and evaluation of the action mechanism of new metallodrugs, transport in the bloodstream and the binding to cellular targets are the key steps. In blood, serum albumins are the most abundant soluble proteins in higher animals and play many crucial physiological functions. These proteins tend to increase the solubility of hydrophobic compounds in plasma and regulate their delivery to target cells. Consequently, properties like absorption, stability, distribution, metabolism and toxicity of the pharmacological active metallocompounds can be significantly affected by their binding to albumins.<sup>3</sup> On the other hand, DNA is the primary target of many metal based anticancer drugs,<sup>4-8</sup> and metal complexes may bind to it leading to alteration and/or inhibition of its functioning.<sup>9,10</sup>

Although considerable attention is paid toward the interaction of metal complexes with biomolecules and their transport processes to the target tissues, their possible transformation in aqueous solution is often not completely taken into account during the design stage and while they are being tested as potential metallic anticancer agents. As for organic drugs the chemical changes are overlooked and it is often assumed that the administered compound reaches the target organs in an unaltered form, the situation is different for metal-based drugs, for which ligand exchange, hydrolysis, chemical bond breaking and redox reactions can occur in the biological media. Therefore, these processes must be taken into account to explain the experimental results. The importance of these transformations have been demonstrated for cisplatin, *cis*-[Pt(NH<sub>3</sub>)<sub>2</sub>Cl<sub>2</sub>], and

oxaliplatin, [Pt(dach)(oxalato)], which, upon hydrolysis, lose the labile chloro and oxalato ligands, respectively, to form the active moiety *cis*-Pt(NH<sub>3</sub>)<sub>2</sub><sup>2+</sup> and Pt(dach)<sup>2+</sup> that interact with DNA.<sup>11,12</sup> A similar situation was also observed with titanocene, Cp<sub>2</sub>TiCl<sub>2</sub>.<sup>13,14</sup> Other studies on Pt-, Au-, Ru- and Rh-based potential drugs pointed in the same direction, identifying the active moieties involved in the ligand exchange or protein-metalation.<sup>15-22</sup> On the other hand, other facts must also be taken into account: polynuclear Au(III), Pd(II), Pt(II) complexes have higher cytotoxicity than mononuclear species,<sup>23-26</sup> and many dimeric and polymeric copper compounds have been described as very promising candidates,<sup>27-30</sup> without considering their possible dissociation in mononuclear units that was demonstrated unambiguously in aqueous solution and coordinating solvents by EPR spectroscopy.<sup>31-35</sup>

Recently, our groups have established that the enhanced protein interaction and cytotoxicity measured for few oxido and non-oxido vanadium complexes are due to the presence of several species in cell media and not (only) for the intact complexes.<sup>36,37</sup> Though the importance of the chemical transformations has been studied for several metals like vanadium (for instance, the anti-diabetic non-oxido V<sup>IV</sup> complexes are active only if they transform into the V<sup>IV</sup>O form which is able to inhibit the protein tyrosine phosphatases<sup>38</sup>), little attention has been paid to the understanding of these factors for molybdenum(VI) complexes.<sup>39</sup>

Potential molybdenum based anticancer agents have been synthesized in oxidation states of +II, +V and +VI over the last few years.<sup>40-45</sup> They could reach the nucleus in an intact form and interact with DNA. Recent studies on the anticancerogenic activity of Mo<sup>VI</sup> complexes have demonstrated that they have a binding affinity toward Calf Thymus DNA (CT DNA), showing a good cytotoxic action on the cell lines HT-29 (human colon cancer) and HeLa (human cervical cancer).<sup>46</sup> Alternatively, the activity of these species can be related to their capability to produce reactive oxygen species (ROS) in solution, which cause cell damages to DNA, lipid peroxidation and cellular signal alteration.<sup>47</sup> Mo<sup>VI</sup> compounds could be reduced in the cellular environment and give

Mo<sup>V</sup> species that are able to form ROS through a Fenton-like reaction  $\text{Mo}^{\text{V}}\text{O}^{3+} + \text{H}_2\text{O}_2 \rightarrow \text{Mo}^{\text{VI}}\text{O}_2^{2+} + \text{H}^+ + \cdot\text{OH}$  and this finding would indicate that Mo<sup>V</sup> could be the active species. Therefore, further experimental investigations on the precise mechanism of the potential molybdenum drugs in solution are needed to exploit their biological activity.

In continuation of our research on the pharmacological properties of various transition metal complexes,<sup>36,46,48-52</sup> herein the synthesis of two monomeric  $[\text{MoO}_2(\text{L}^1)(\text{MeOH})]$  (**1**),  $[\text{MoO}_2(\text{L}^2)(\text{EtOH})]$  (**2**) and two mixed-ligand dimeric  $[\{\text{MoO}_2(\text{L}^{1-2})\}_2(\mu\text{-4,4'-bipy})]$  (**3** and **4**) dioxidomolybdenum(VI) complexes from two aroylhydrazone ligands ( $\text{H}_2\text{L}^{1-2}$ ) are reported. The complexes revealed a distorted octahedral geometry with the sixth labile coordination site occupied by the solvent molecule (MeOH/EtOH) in case of the monomeric complexes and the co-ligand 4,4'-bipyridine in case of the dimeric complexes.<sup>53-55</sup> Hydrazones are important set of ligands, as they manifests a vast range of pharmaceutical activities.<sup>56-59</sup> It has been demonstrated that their biological properties are considerably enhanced upon complexation to metal ions.<sup>60</sup> Moreover, the incorporation of co-ligands with powerful  $\sigma$  donor functions, such as 4,4'-bipyridine might affect the planarity, hydrophobicity, and general anticancer action of metal complexes.<sup>61,62</sup> The interaction of the synthesized compounds with human serum albumin (HSA) and CT-DNA has been studied with the combined application of instrumental and computational methods. Further, studies on their redox properties and capability to produce ROS were also carried out. Finally, the Mo complexes were screened for their anticancer activity against human cervical cancer (HeLa) and human colon cancer (HT-29) and noncancerous mouse embryonic fibroblast (NIH-3T3) cell lines. In order to assess their potential anticancer mechanism, apoptotic activity, and cell cycle analysis were also carried out. Notably, the results can be related to the transformation of **1-4** in biological media and allow to discuss the importance of the chemical changes in the explanation of the pharmacological activity of metal-based potential drugs.

## EXPERIMENTAL AND COMPUTATIONAL SECTION

### Materials and methods

Reagent grade solvents used in the study were dried and distilled prior to use. All chemicals were commercially procured and used as received.  $[\text{Mo}^{\text{VI}}\text{O}_2(\text{acac})_2]$  was prepared as described earlier.<sup>63</sup> Reagents for biological assays were procured mostly from HiMedia laboratories and Sigma Aldrich (USA).

Elemental analyses were performed on a VarioELcube CHNS Elemental analyzer.

ESI-MS spectra were recorded in the positive-ion mode on an SQ-300 MS instrument operating in ESI mode or on a Thermo Fisher Scientific Q Exactive™ Plus Hybrid Quadrupole-Orbitrap™ spectrometer. The solutions were infused at a flow rate of 5.00  $\mu\text{L}/\text{min}$  into the ESI chamber and the spectra were obtained in the  $m/z$  range 150-2000 with a resolution of 140,000 and accumulated for at least 5 min to increase the signal-to-noise ratio. The instrumental settings were: spray voltage 2,300 V, capillary temperature 250 °C, sheath gas 10 (arbitrary units), auxiliary gas 3 (arbitrary units), sweep gas 0 (arbitrary units), probe heater temperature 50 °C. The spectra were measured after dissolving the solid Mo complexes **1-4** in LC-MS grade solvent (MeOH, MeOH/H<sub>2</sub>O 90/10 v/v or CH<sub>3</sub>CN) to obtain a concentration of 45-50  $\mu\text{M}$ .<sup>a</sup> Spectra were analyzed by using Thermo Xcalibur 3.0.63 software (Thermo Fisher Scientific).

IR and UV spectra were recorded on a Perkin-Elmer Spectrum RXI and Perkin-Elmer Lambda 25, Lambda 35 or Varian Cary 1E spectrophotometers, respectively.

NMR spectra were recorded on a Bruker Ultrashield 400 MHz spectrometer at 298 K room temperature using SiMe<sub>4</sub> (<sup>1</sup>H and <sup>13</sup>C) as an internal standard.

EPR spectra were recorded at room temperature using a Bruker AquaX cell with an X-band Bruker EMX spectrometer equipped with a HP 53150A microwave frequency counter. The microwave

---

<sup>a</sup> In the manuscript, all the concentrations of the Mo complexes are given based on their molar concentration.

frequency was 9.83-9.85, microwave power was 20 mW, time constant was 81.92 ms, modulation frequency 100 kHz, modulation amplitude 0.4 mT, resolution 4096 points.

### Synthesis of ligands

The aroylhydrazone ligands,  $H_2L^{1-2}$ , were prepared by the condensation of 4-diethyl amino salicylaldehyde with its corresponding hydrazides (2-furoic hydrazide and thiophene 2-carboxylic hydrazide) in a slightly acidic ethanolic medium for 2 h. The resulting yellowish white compounds were filtered, washed with ethanol and dried over fused  $CaCl_2$ .

**$H_2L^1$** : Yield: 0.24 g (70%). Anal. Calcd for  $C_{16}H_{19}N_3O_3$ : C, 63.77; H, 6.36; N, 13.94. Found: C, 63.72; H, 6.39; N, 13.91%. FTIR (KBr,  $\nu_{max}/cm^{-1}$ ):  $\nu(O-H)$  3214,  $\nu(N-H)$  2972,  $\nu(C=O)$  1634,  $\nu(C=N)$  1592.  $^1H$  NMR (400 MHz,  $DMSO-d_6$ ):  $\delta$  (ppm) = 11.83 (s, 1H,  $-NH$ ), 11.32 (s, 1H,  $-OH$ ), 8.41 (s, 1H,  $-CH$ ), 7.94–6.11 (m, 6H, aromatic), 3.36 (q, 4H,  $-CH_2$ ), 1.10 (t, 6H,  $-CH_3$ ).  $^{13}C$  NMR (100 MHz,  $DMSO-d_6$ ):  $\delta$  (ppm) = 162.87, 160.15, 157.89, 152.65, 144.66, 140.56, 128.06, 126.31, 118.24, 116.31, 108.46, 99.67, 45.32, 14.65.

**$H_2L^2$** : Yield: 0.22 g (74%). Anal. Calcd for  $C_{16}H_{19}N_3O_2S$ : C, 60.54; H, 6.03; N, 13.24; S, 10.10. Found: C, 60.59; H, 6.08; N, 13.20; S, 10.02%. FTIR (KBr,  $\nu_{max}/cm^{-1}$ ):  $\nu(O-H)$  3204,  $\nu(N-H)$ , 2969,  $\nu(C=O)$  1630,  $\nu(C=N)$  1598.  $^1H$  NMR (400 MHz,  $DMSO-d_6$ ):  $\delta$  (ppm) = 11.82 (s, 1H,  $-NH$ ), 11.47 (s, 1H,  $-OH$ ), 8.37 (s, 1H,  $-CH$ ), 8.23–6.11 (m, 6H, aromatic), 3.33 (q, 4H,  $-CH_2$ ), 1.08 (t, 6H,  $-CH_3$ ).  $^{13}C$  NMR (100 MHz,  $DMSO-d_6$ ):  $\delta$  (ppm) = 163.87, 160.07, 154.26, 150.65, 142.66, 138.56, 129.06, 119.72, 115.26, 112.12, 105.54, 98.82, 45.49, 13.24.

### Synthesis of complexes 1–2

$MoO_2(acac)_2$  (1 mmol) was added to an alcoholic solution of ligand  $H_2L^{1-2}$  (1 mmol). The earlier yellow solution containing the ligand immediately turned into dark red after the addition of the metal precursor. The solution was allowed to reflux for 3 h. Thereafter the solution was filtered and dark red crystals suitable for X-ray analysis was produced upon its slow evaporation over 2 days.

**[MoO<sub>2</sub>(L<sup>1</sup>)(MeOH)] (1):** Yield: 0.22 g (65 %). Anal. Calcd for C<sub>34</sub>H<sub>42</sub>Mo<sub>2</sub>N<sub>6</sub>O<sub>12</sub>: C, 44.45; H, 4.61; N, 9.15. Found: C, 44.50; H, 4.58; N, 9.10%. FTIR (KBr,  $\nu_{\max}/\text{cm}^{-1}$ ):  $\nu(\text{C}=\text{N})$  1609,  $\nu(\text{M}=\text{O})$  934, 917. UV-Vis (DMSO):  $\lambda_{\max}$ , nm ( $\epsilon$ ,  $\text{dm}^3 \text{mol}^{-1} \text{cm}^{-1}$ ): 473 (6777), 355 (9378). <sup>1</sup>H NMR (400 MHz, DMSO-*d*<sub>6</sub>):  $\delta$  (ppm) = 8.50 (s, 1H, -CH), 7.77–6.13 (m, 6H, aromatic), 4.37 (1H, OH methanol), 3.94 (s, 3H, -CH<sub>3</sub> methanol), 3.34 (q, 4H, -CH<sub>2</sub>), 1.09 (t, 6H, -CH<sub>3</sub>). <sup>13</sup>C NMR (100 MHz, DMSO-*d*<sub>6</sub>):  $\delta$  (ppm) = 162.53, 161.28, 155.77, 152.58, 135.59, 133.83, 131.89, 130.49, 124.66, 108.80, 105.58, 98.56, 56.65, 44.46, 13.12.

**[MoO<sub>2</sub>(L<sup>2</sup>)(EtOH)] (2):** Yield: 0.23 g (68 %). Anal. Calcd for C<sub>18</sub>H<sub>23</sub>MoN<sub>3</sub>O<sub>5</sub>S: C, 44.18; H, 4.74; N, 8.59; S, 6.55. Found: C, 44.10; H, 4.77; N, 8.50; S, 6.58%. FTIR (KBr,  $\nu_{\max}/\text{cm}^{-1}$ ):  $\nu(\text{C}=\text{N})$  1614,  $\nu(\text{M}=\text{O})$  941, 918. UV-Vis (DMSO):  $\lambda_{\max}$ , nm ( $\epsilon$ ,  $\text{dm}^3 \text{mol}^{-1} \text{cm}^{-1}$ ): 478 (7207), 360 (8721). <sup>1</sup>H NMR (400 MHz, DMSO-*d*<sub>6</sub>):  $\delta$  (ppm) = 8.58 (s, 1H, -CH), 7.88–6.14 (m, 6H, aromatic), 4.38 (1H, OH<sub>ethanol</sub>), 3.46 (q, 4H, -CH<sub>2</sub>), 3.43 (q, 2H, -CH<sub>2</sub><sub>ethanol</sub>), 1.11 (t, 6H, -CH<sub>3</sub>), 1.06 (t, 3H, -CH<sub>3</sub><sub>ethanol</sub>). <sup>13</sup>C NMR (100 MHz, DMSO-*d*<sub>6</sub>):  $\delta$  (ppm) = 162.83, 161.63, 154.87, 153.58, 135.91, 133.93, 131.24, 130.49, 128.66, 108.87, 106.58, 99.56, 56.50, 44.59, 19.03, 13.01.

### Synthesis of complexes 3–4

MoO<sub>2</sub>(acac)<sub>2</sub> (1 mmol) was added to an acetonitrile solution of ligand H<sub>2</sub>L<sup>1-2</sup> (1 mmol), followed by the addition of 4,4'-bipyridine. The earlier yellow solution containing the ligand immediately turned into dark red after the addition of the metal precursor and the co-ligand. The solution was allowed to reflux for 3 h. Thereafter the solution was filtered and dark red crystals suitable for X-Ray analysis was produced upon its slow evaporation over 2 days.

**[[MoO<sub>2</sub>(L<sup>1</sup>)]<sub>2</sub>( $\mu$ -4,4'-bipy)] (3):** Yield: 0.32 g (55 %). Anal. Calcd for C<sub>42</sub>H<sub>42</sub>Mo<sub>2</sub>N<sub>8</sub>O<sub>10</sub>: C, 49.91; H, 4.19; N, 11.09. Found: C, 49.88; H, 4.15; N, 11.12%. FTIR (KBr,  $\nu_{\max}/\text{cm}^{-1}$ ):  $\nu(\text{C}=\text{N})$  1618,  $\nu(\text{M}=\text{O})$  934, 927. UV-Vis (DMSO):  $\lambda_{\max}$ , nm ( $\epsilon$ ,  $\text{dm}^3 \text{mol}^{-1} \text{cm}^{-1}$ ): 475 (6052), 356 (8154). <sup>1</sup>H NMR (400 MHz, DMSO-*d*<sub>6</sub>):  $\delta$  (ppm) = 8.73 (s, 1H, -CH), 8.58–6.14 (m, 10H, aromatic) 3.40 (q,



4H, -CH<sub>2</sub>), 1.11 (t, 6H, -CH<sub>3</sub>). <sup>13</sup>C NMR (100 MHz, DMSO-*d*<sub>6</sub>): δ (ppm) = 161.68, 159.26, 155.39, 153.64, 151.02, 146.38, 145.56, 144.79, 135.96, 122.02, 121.77, 118.56, 114.86, 112.69, 108.83, 106.59, 99.58, 44.59, 13.00.

**[[MoO<sub>2</sub>(L<sup>2</sup>)]<sub>2</sub>(μ-4,4'-bipy)] (4)**: Yield: 0.29 g (52 %). Anal. Calcd for C<sub>42</sub>H<sub>42</sub>Mo<sub>2</sub>N<sub>8</sub>O<sub>8</sub>S<sub>2</sub>: C, 48.37; H, 4.06; N, 10.75; S, 6.15. Found: C, 48.30; H, 4.02; N, 10.64; S, 6.13%. FTIR (KBr, ν<sub>max</sub>/cm<sup>-1</sup>): ν(C=N) 1589, ν(M=O) 936, 920. UV-Vis (DMSO): λ<sub>max</sub>, nm (ε, dm<sup>3</sup> mol<sup>-1</sup> cm<sup>-1</sup>): 479 (9226), 358 (11269). <sup>1</sup>H NMR (400 MHz, DMSO-*d*<sub>6</sub>): δ (ppm) = 8.75 (s, 1H, -CH), 8.56–6.16 (m, 10H, aromatic) 3.38 (q, 4H, -CH<sub>2</sub>), 1.10 (t, 6H, -CH<sub>3</sub>). <sup>13</sup>C NMR (100 MHz, DMSO-*d*<sub>6</sub>): δ (ppm) = 161.66, 159.54, 156.07, 153.52, 150.74, 146.35, 145.31, 143.61, 137.94, 124.01, 120.51, 117.11, 115.59, 111.94, 109.22, 106.58, 99.56, 44.55, 13.15.

## Crystallography

Suitable single crystals for X-ray diffraction study of the complexes (**1–4**) were mounted on a mylar loop in oil. Data were collected using a STOE IPDS 2 diffractometer equipped with an Oxford Cryosystems low-temperature device operating at T = 250(2) K. Crystallographic data and details of refinement for all the complexes are listed in **Table S1**. Data were measured using rotation method using MoKα radiation. The structure was solved with the **ShelXT**<sup>64</sup> solution program using dual methods and by using **Olex2**<sup>65</sup> as the graphical interface. The model was refined with **ShelXL**<sup>64</sup> using full matrix least squares minimisation on *F*<sup>2</sup>. All non-hydrogen atoms were refined anisotropically. Hydrogen atom positions were calculated geometrically and refined using the riding model. Hydrogen atom positions were calculated geometrically and refined using the riding model.

The disorders of the complexes were refined by SIMU and DELU commands. These restraints were introduced to improve displacement parameters of methyl moieties and the oxygen atoms bonding to Mo2 in complex **1**. As for the rest complexes, the displacement parameters of partially overlapping atoms of the disordered moiety were stabilized with SIMU and DELU commands.

Additional DFIX and DELU restraints were introduced to optimize ethyl moieties in complex **2**. The proton on O5 was refined with fixed bond distance of 0.87 Å.

### DFT Calculations

The geometry of the monomeric  $[\text{Mo}^{\text{VI}}\text{O}_2(\text{L}^{1-2})]$ ,  $[\text{Mo}^{\text{VI}}\text{O}_2(\text{L}^{1-2})(\text{Ac})]^-$ ,  $[\text{Mo}^{\text{VI}}\text{O}_2(\text{L}^{1-2})(\text{MeIm})]$  and dimeric  $[\{\text{MoO}_2(\text{L}^{1-2})\}_2(\mu\text{-4,4'-bipy})]$  complexes were optimized with Gaussian09<sup>66</sup> at DFT theory level using the hybrid B3LYP functional combined with Grimme's D3 correction<sup>67</sup> for dispersion; the split-valence plus polarization functions 6-31g(d,p) basis set was applied for the main group elements, while SDD plus *f*-functions<sup>68</sup> and pseudopotential for Mo. The effect of solvation was taken into account using the SMD continuum model of Marenich *et al.* for water and methanol.<sup>69</sup> For all the structures, minima were verified through frequency calculations.

The thermodynamic stability in solution was estimated computing the Gibbs free energy change in implicit solvent continuum model.<sup>70</sup> The final Gibbs free energies were obtained by addition of the thermal and entropic corrections ( $G^{\text{therm}}$ ), obtained in the optimization stage, to the potential energy of single point calculations with the extended basis-set *def2-TZVP* for the main group elements<sup>70</sup> and the quadruple- $\zeta$  *def2-QZVP* basis set for Mo.<sup>71</sup>

### Serum bioligand binding assays

Solutions containing **1** or **2** and a serum bioligand (citrate, lactate and histidine) were prepared in mixtures H<sub>2</sub>O/MeOH 90/10 v/v (for **1**), H<sub>2</sub>O/MeOH 80/20 v/v (for **2**) or H<sub>2</sub>O/MeOH 50/50 v/v (for both of them). Citric acid (citr) was purchased from Fluka (code 27490) L-lactic acid (lact) from Sigma (code L1750), L-histidine (His) from J. T. Baker (code 1603). The molar ratio was 1/1, Mo concentration 50 or 10 μM and pH 7.4 or 5.0. Electronic absorption spectra were recorded immediately after the preparation of the solutions at room temperature.

### HSA binding assays

The experiments concerning the binding of the complexes with protein were performed with fatted human serum albumin (HSA) (Sigma, A9511) in 50 mM Tris-HCl buffer (pH 7.4) containing 10%

DMF.<sup>72</sup> Concentration of HSA stock solution was determined by taking its molar absorption coefficient at 278 nm ( $35700 \text{ M}^{-1} \text{ cm}^{-1}$ ) through UV absorbance.<sup>73</sup> The solution was preserved at 4 °C in the dark and used within 4 days of its preparation.

#### *Fluorescence quenching study of the complexes with HSA protein*

Interaction of the synthesized complexes with HSA was investigated through fluorescence quenching experiments. The emission spectra were recorded at 345 nm and excitation wavelength at 280 nm by addition of an increasing concentration of complex **1–2** (0–100  $\mu\text{M}$ ) and **3–4** (0–300  $\mu\text{M}$ ) to a fixed concentration of HSA (10  $\mu\text{M}$ ) with a Fluoromax 4P spectrofluorimeter (Horiba Jobin Mayer, USA) at room temperature.

#### *Molecular docking on HSA*

Docking calculations to HSA were carried out through GOLD 5.8 software,<sup>74</sup> according to the procedures recently reported.<sup>37,75–82</sup> The XRD structure of albumin crystallized in presence of stearic acid was used as a model for fatted HSA (PDB code: 1E7I).<sup>83</sup> The PDB structure was cleaned removing all the crystallographic waters, and hydrogen atoms were added with the UCSF Chimera program.<sup>84</sup> Based on the DFT results, only classical dockings were carried out, in which the complex  $[\text{Mo}^{\text{VI}}\text{O}_2(\text{L}^1)]$  can bind only through second coordination sphere interactions. The blind exploration was performed on the rigid protein building four evaluation spheres of 20 Å containing globally the whole protein. Genetic algorithm (GA) parameters have been set in 50 GA runs and a minimum of 100,000 operations. The other parameters of GA were set to default. The scoring (*Fitness* of GoldScore) was determined through the recent validated versions of GoldScore accounting for metal-complexes surface interactions.<sup>78</sup> The best solutions (binding poses) were evaluated taking into account the mean ( $F_{\text{mean}}$ ) and the highest value ( $F_{\text{max}}$ ) of the scoring and population of the cluster containing the best pose.

#### *Förster resonance energy transfer (FRET)*

$R_0$  value was calculated with the help of eq. (1).<sup>85,86</sup>

$$R_0 = 0.02108 \left( K^2 \Phi_D \eta^{-4} J \right)^{1/6} \quad (1)$$

In the above equation (eq. (1)), the orientation factor between the emission dipole of the donor and the absorption dipole of the acceptor  $K^2$  is taken as 2/3, the fluorescence quantum yield of the donor  $\Phi_D$  is 0.118, refractive index of the medium  $\eta$  is 1.33 and  $J$  is the extent of spectral overlap of the donor (HSA) emission and the acceptor (complex) absorption spectra.<sup>86</sup> The resonance transfer is more efficient when the spectral overlap of the emission spectrum of the donor molecule and the absorption spectrum of the acceptor molecule is large.<sup>87</sup>

The values of the parameter  $J$  were calculated by using eq. (2):<sup>85,86</sup>

$$J = \int \bar{I}_D(\lambda) \epsilon_A \lambda^4 d\lambda \quad (2)$$

In eq. (2),  $\lambda$  represents the wavelength,  $\bar{I}_D(\lambda)$  is the normalized fluorescence emission of the donor HSA at the wavelength  $\lambda$  and  $\epsilon_A(\lambda)$  is the molar extinction coefficient of the acceptor metal complex at wavelength  $\lambda$ .

### **DNA binding assays**

All the experiments concerning the binding of the complexes with DNA were performed with calf-thymus DNA (CT DNA, Sigma, D1501) in 50 mM Tris-HCl buffer (pH 7.4) containing 10% DMF.<sup>72</sup> The concentration of the stock solutions of CT DNA was calculated from its absorption intensity at 260 nm with a molar extinction coefficient of 6600 M<sup>-1</sup> cm<sup>-1</sup>,<sup>88</sup> its ratio of 1.8–1.9 for

UV absorbance at 260 nm and 280 nm indicated that the DNA was sufficiently protein free. CT DNA was stored at 4 °C and utilized within 4 days of preparation.

#### *Absorption Titration*

The UV–Vis absorption titration experiments were performed in order to examine the binding affinity of the Mo complexes (**1–4**) with CT DNA. A fixed concentration of the complex **1–2** (10  $\mu$ M) and **3–4** (30  $\mu$ M) was titrated along with increasing concentrations of CT DNA (0–100  $\mu$ M). An equal volume of CT DNA was added to the blank solution cuvette to eliminate its absorbance. The solutions were allowed to incubate at room temperature for 5 min before recording the related spectra.

#### *Competitive DNA binding fluorescence measurements*

The competitive binding experiments were performed as described earlier against various DNA binding probes namely ethidium bromide (EB), 4',6-diamidino-2-phenylindole (DAPI) and methyl green (MG). As DAPI and MG bind to minor and major groove of the DNA, respectively, and EB bind to DNA by intercalation, their displacement from DNA leading to a quench in the fluorescent intensity may be an indication of the binding mode of the tested complexes.<sup>49,89</sup>

In brief, DNA binding probe *i.e.* EB, DAPI or MG was allowed to incubate with CT DNA in 50 mM Tris–HCl buffer (pH 7.4) containing 10% DMF<sup>72</sup> at room temperature for 30 min. Subsequently, the fluorescence intensities of the complexes **1–4** was measured with DAPI, MG and EB bound CT DNA with increasing concentration of the Mo complexes (0–100  $\mu$ M). The fluorescence emission intensities of EB, DAPI and MG was monitored at 597 nm (excitation 510 nm), 455 nm (excitation 358 nm), and 672 nm (excitation 633 nm) with a Fluoromax 4P spectrofluorimeter (Horiba Jobin Mayer, USA).

#### *Circular Dichroism Study*

Circular Dichroism experiment was performed as described earlier.<sup>49,89</sup> Briefly, spectra of CT DNA (100  $\mu$ M) was recorded in the absence and presence of complexes **1–2** (25  $\mu$ M) and **3–4** (75  $\mu$ M) at

25 °C in the wavelength range of 240–400 nm using a JASCO J-1500 CD spectrophotometer. All the experiments were performed in a 50 mM Tris–HCl buffer (pH 7.4) containing 10% DMF using a quartz cell with 10 mm path length.<sup>72</sup>

#### *Molecular docking on DNA*

Docking calculations to DNA were carried out through GOLD 5.8 software,<sup>73</sup> according to the procedures recently reported.<sup>37,75–82</sup> The NMR solution of DNA adduct with pyrrolo[2,1-c][1,4]benzodiazepine was used as a model for CT-DNA after removing the bound substrate (PDB code: 2K4L<sup>90</sup>). Based on the binding assays and DFT results, only classical dockings were carried out, in which the complex  $[\text{Mo}^{\text{VI}}\text{O}_2(\text{L}^1)]$  can bind only through second coordination sphere interactions. The blind exploration was performed on the rigid DNA, building one evaluation sphere of 20 Å containing globally the whole structure. GA parameters have been set to 50 runs and a minimum of 100,000 operations, while the other parameters were set to default. The best solutions (binding poses) were evaluated taking into account the mean ( $F_{\text{mean}}$ ) and highest value ( $F_{\text{max}}$ ) of the GoldScore and the population of the cluster containing the best pose.

#### **Cytotoxicity activity and mechanism of action**

##### *Cell culture*

In the present study, two cancer cell lines, that are human cervical cancer (HeLa) and human colon cancer (HT-29) and noncancerous mouse embryonic fibroblast (NIH-3T3) cell lines, were used. These cell lines were purchased from NCCS, Pune, India. The cells were maintained in Dulbecco's Modified Eagle Media (DMEM) supplemented with fetal bovine serum (FBS) and antibiotics at 37 °C in a humidified incubator (5% CO<sub>2</sub>) with regular passaging.

##### *Determination of the cytotoxic potential*

The cytotoxic potential of the complexes **1–4** was determined against the above cell lines through a conventional MTT [3-(4,5-dimethylthiazol-2-yl)-2,5-diphenyltetrazoliumbromide] inspection.<sup>48,49,51,91</sup> Briefly, after the cells attained 80% confluency, the cells were seeded in a 96

well plate at a concentration of  $5 \times 10^4$  cells per well. These cells were then treated for a period of 48 h, with different concentrations of each complex that was initially dissolved in DMSO and further diluted in DMEM media. Final working concentration of DMSO was maintained at less than 0.1% (v/v). Untreated cells were taken for control group experiment. After the treatment period, 20  $\mu$ L of MTT (5 mg/mL in PBS) solution was added to each well and incubated for 3 h. Subsequently, 200  $\mu$ L of DMSO was added to each well and further incubated for 30 min before measuring the absorbance in a spectrophotometer at 595 nm. Cytotoxicity was evaluated by the IC<sub>50</sub> value (concentration of the complex inhibiting 50% of cell growth with respect to the control) for each complex.

#### *Reduction by cellular reductants*

The tendency of the examined Mo complexes to be reduced and complexed in the cytosol has been studied in solutions containing L-ascorbic acid (Asc) and reduced glutathione (GSH) through the combined application of EPR, ESI-MS and UV-Vis techniques. Asc was purchased from Honeywell Riedel-de Haen (code 33034) and GSH from Sigma-Aldrich (code G4251).

For EPR spectra, a 20 mM solution of L-ascorbic acid in PBS (pH 7.4) was prepared; subsequently, different solutions containing Asc and the complexes **1–4** with variable ratios ranging from 1/1 to 10/1 (Asc/**1–4**) were studied in mixtures PBS/DMSO 1/1 (v/v). Similarly, a 20 mM GSH solution was prepared in PBS (pH 7.4) and solutions containing different ratios GSH/**1–4** ranging from 1/1 to 10/1 were examined in mixtures PBS/DMSO 1/1 (v/v). After the preparation of the solutions, EPR spectra were recorded at room temperature using an AquaX cell.

For ESI-MS experiments, solutions containing **1** and Asc or GSH were prepared in a mixture MeOH/H<sub>2</sub>O 90/10 v/v with molar ratio 1/1 and 1/10 and Mo concentration 5 or 50  $\mu$ M.

For electronic absorption spectra measurements, solutions containing **1** and **2** with Asc or GSH were prepared in mixtures H<sub>2</sub>O/MeOH 90/10 v/v (for **1**) or H<sub>2</sub>O/MeOH 80/20 v/v (for **2**) with a molar ratio of 1/1, Mo concentration of 50  $\mu$ M and pH 7.4 or 5.0.

### *DMPO assay*

The capability of Mo<sup>VI</sup> compounds to produce hydroxyl radicals  $\cdot\text{OH}$  by Fenton-like reactions in presence of reducing agents was studied with the 5,5-dimethyl-1-pyrroline *N*-oxide (DMPO) assay on complexes **1–4**. In this assay  $\cdot\text{OH}$  radicals eventually generated in solution are trapped by a spin trap (DMPO) to form a stable radical adduct (DMPO–OH) which can be detected by EPR measurements.

Solutions containing H<sub>2</sub>O<sub>2</sub> (1 mM), DMPO (600  $\mu\text{M}$ ) and Mo<sup>VI</sup> complex (**1–4**, 10  $\mu\text{M}$ ) in presence or not of reducing agents (GSH or ascorbate, 100  $\mu\text{M}$ ) were prepared. Aqueous stock solutions of H<sub>2</sub>O<sub>2</sub>, DMPO, GSH and Asc were used, while solutions with **1–4** were prepared in DMSO. EPR spectra were recorded at room temperature after the preparation of the mixture reactions using a Bruker AquaX capillary cell.

### *Nuclear staining*

The status of nuclear disintegration in cancerous cells in response to complex treatment was examined by staining with DAPI.<sup>48,49,51,91</sup> HeLa and HT-29 cells were treated with IC<sub>50</sub> concentration of the complexes. Complexes were not added to cells for control group experiment. After 12 h of treatment, 4% paraformaldehyde solution was added to both control and treated cells. Thereafter, the above fixed cells were stained with DAPI. The cells were then examined under fluorescence microscope (Olympus IX 71).

### *Cell Cycle Analysis*

HeLa ( $5 \times 10^5$  cells per well) were grown in a 6-well plate suspended in 2 mL of DMEM medium under previously described culturing conditions. The cells were then treated with different concentrations of the complexes for 24 h. Post treatment, cells were harvested as pellets and fixed using an ice-cold 70% ethanolic solution at  $-20\text{ }^\circ\text{C}$  overnight. Further, the cells were washed twice with ice-cold PBS, and then re-suspended in  $1 \times$  PBS solution containing PI ( $10\text{ }\mu\text{g mL}^{-1}$ ) and



RNaseA ( $10 \mu\text{g mL}^{-1}$ ) solution. The cell suspension was gently mixed and incubated for 30 min at  $37^\circ\text{C}$  in the dark. Cell cycle was analyzed using a BD Accuri C6 flow cytometer<sup>92</sup>

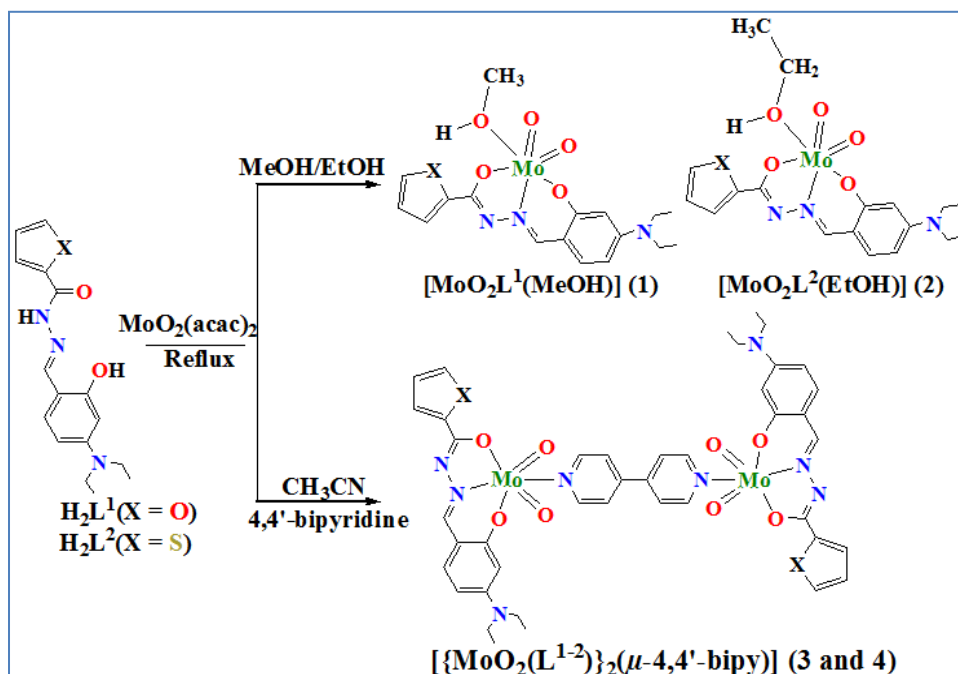
#### *Cell apoptosis assay*

Analysis of apoptotic populations of HeLa cells induced by the complexes (**1–4**) were determined by Annexin V and PI staining according to the manufacturer's protocol for the Annexin V: FITC Apoptosis Detection Kit (Abgenex) by flow cytometry. In brief, the cells were treated with the complexes for a period of 48 h. After drug exposure, cells were collected by centrifugation, and washed with PBS. The cells were then re-suspended in  $100 \mu\text{l}$  of Annexin V-FITC 1X binding buffer. The cell suspension was incubated at room temperature in the dark for 15 min after mixing with  $4 \mu\text{l}$  of Annexin V-FITC and  $4 \mu\text{l}$  of PI. Subsequently, the samples were analyzed by a BD Accuri C6 flow cytometer.<sup>93</sup>

## **RESULTS AND DISCUSSION**

### **Synthesis**

The synthetic procedure of **1–4** from two aroylhydrazone ligands containing a diethylamine substituent is represented in **Scheme 1**. Upon reaction of  $\text{H}_2\text{L}^{1-2}$  with  $\text{MoO}_2(\text{acac})_2$  in alcoholic medium, deep red crystals of **1** and **2** were obtained from slow evaporation of the filtrate, while the addition of 4,4'-bipyridine as a co-ligand in acetonitrile medium to the above reaction mixture yielded reddish brown crystals of **3** and **4** directly from the reflux conditions.



**Scheme 1** Schematic representation for the synthesis of  $[MoO_2(L^1)(MeOH)]$  (1),  $[MoO_2(L^2)(EtOH)]$  (2), and  $[{MoO_2(L^{1-2})}_2(\mu-4,4'-bipy)]$  (3 and 4).

### X-ray structure description

In order to predict a specific coordination mode of  $H_2L^{1-2}$  or stereochemistry for the monomeric  $Mo^{VI}$  complexes, the structures of **1–4** were determined through X-ray crystallography. The crystal data and structure refinement details are given in **Table S1**. The solid state structures of the complexes **1** and **2** are shown in **Figure 1** and **S1** and the selected bond lengths and bond angles are enlisted in **Tables S2** and **S3**.

The crystal lattice of complex **1** is composed of two units with identical coordination geometry, differing only in the position of the alkyl chains. The structures of **1** and **2** (**Figures 1** and **S1**) reveal that the ligand is coordinated to  $Mo^{VI}O_2^{2+}$  ion as an O,N,O-donor, with bite angles of  $\sim 71^\circ$  and  $\sim 82^\circ$  for O(1)–Mo(1)–N(2) and O(2)–Mo(1)–N(2), respectively (**Tables S2** and **S3**). Further, a solvent molecule is also coordinated to the metal center in *trans* to one Mo=O bond; therefore, the complex can be formulated as  $[MoO_2(L^1)(MeOH)]$

(1)  $[\text{MoO}_2(\text{L}^2)(\text{EtOH})]$  (2) where L refers to an aroylhydrazone ligand. This composition is found to be consistent with the microanalytical data. In these structures, the coordination geometry around molybdenum center can be described as distorted octahedral as given in the bond parameters around the metal center. A solvent molecule like methanol and ethanol completes the distorted octahedral coordination sphere of **1** and **2** respectively and provides stability to the system in solid state. The Mo=O, Mo–O, Mo–N, C=N and N–N bond lengths are within the normal range for  $\text{Mo}^{\text{VI}}\text{-L}$  fragment.<sup>94–98</sup> The longer bond length of Mo–O(Solv) found in these complexes in comparison to the normal single bond length [2.354(3) Å against 1.932(3)–2.024(3) Å], indicates a weak site available for ligand substitutions (Tables S2 and S3). This feasibility is realized in the facile formation of adducts with formula  $[\{\text{MoO}_2(\text{L}^{1-2})\}_2(\mu\text{-4,4'-bipy})]$  (**3** and **4**).

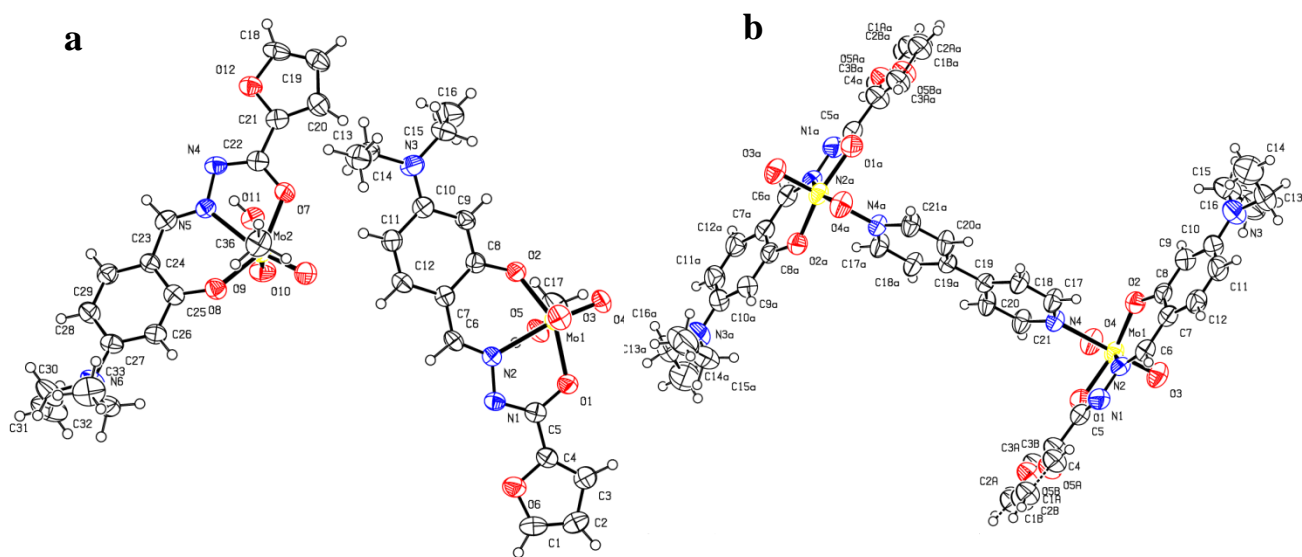


**Figure 1** Molecular structures of the complex **1** (a) and **3** (b) with atomic numbering scheme used.

On the other hand, the dimeric complexes [ $\{\text{MoO}_2(\text{L}^{1-2})\}_2(\mu\text{-}4,4'\text{-bipy})$ ] (**3** and **4**, **Figures 1** and **S1**) crystallize in orthorhombic crystal system and *Pbca* space group, while the molecule is present in a crystallographic center of inversion. Each half of the dimeric structure is identical to the other one. There is a distorted octahedral coordination environment around the  $\text{Mo}^{\text{VI}}$  center, where the dianionic and tridentate ligand  $(\text{L}^{1-2})^{2-}$  with its meridionally situated donors O(1), N(2) and O(2) lay in the equatorial plane along with the oxido ligand O(3) for **3** and O(4) for **4**. The Mo–O distances range from 1.700(3)–1.698(4) Å for the oxido ligand O(4) for **3** and O(3) for **4**, located in an axial position, and 1.912(3)–1.921(3) Å for the phenolato oxygen O(2). The Mo(1)–O(1)(enolato) distance is 2.001(3)–2.007(4) Å, while the second axial position is held by a nitrogen atom of the bridging 4,4'-bipyridine ligand, and is observed to be significantly further from the Mo center than the other five ligated atoms. Mo(1)–N(4), at 2.420(3)–2.421(4) Å, is the most long of all the six Mo–L bonds and, therefore, the most susceptible to ligand exchange.<sup>96</sup> The chelate bite angles for the five- and six-membered rings have values within the expected ranges [O(2)–Mo(1)–N(2), 81.83(14)°; O(1)–Mo(1)–N(2), 71.57(14)°] (**Table S3**).

### Spectral characteristics

Spectral characteristics of the ligands ( $\text{H}_2\text{L}^{1-2}$ ) and complexes **1–4** have been listed in the *Experimental and Computational Section*. FT-IR spectra of the complexes exhibit two stretching bands in the range 917–941  $\text{cm}^{-1}$ , indicating the dioxido nature of  $\text{MoO}_2^{2+}$  ion.<sup>50,95,99</sup> Electronic spectra of **1–4** display strong or moderate intensity bands in the range 473–479 nm and 355–360 nm due to ligand to metal charge transfer (LMCT) and ligand centered transitions, respectively.<sup>50,95,99</sup> The representative absorbance spectrum of **2** is given in **Figure S2**. In comparison to the signals of the ligands, NMR spectra of the complexes show a disappearance of –OH and –NH protons due to deprotonation and

coordination of the metal atom. Monomeric complexes **1** and **2** exhibit additional peaks in the expected region for the axially coordinated MeOH and EtOH molecule respectively. Besides, there is an increased number of resonances in the aromatic region for the dimeric complex **3** and **4** as compared to its free ligands  $H_2L^{1-2}$  which is due to the coordinated co-ligand 4,4'-bipy. Due to crystallographic center of inversion, resonance peaks of only one half of the molecule are visible in the spectra.

The  $^{13}C$  NMR signals of the complexes, as listed in the *Experimental and Computational Section*, confirm that the coordinated labile solvent molecule (alcohol) for **1** and **2** remains coordinated in an organic solvent like DMSO. In the downfield region ( $\delta = 156.07-99.56$  ppm) an increased number of aromatic carbon peaks for complexes **3** and **4**, in comparison to their corresponding ligand backbone, confirm the presence of the 4,4'-bipy co-ligand in the vicinity of the metal and also supports that the two structurally characterized dimeric complexes retain their identity in DMSO.

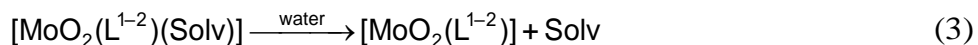
### **Stability in aqueous solution: spectroscopic/spectrometric behavior and DFT calculations**

The stability of all the complexes has been established in water through UV-Vis spectroscopy, ESI mass spectrometry and DFT methods. The electronic absorption spectra recorded as a function of the time on **1–4** in 50 mM Tris–HCl buffer (pH 7.4) containing 10% DMF are depicted in **Figure S3**. The first thing that must be noticed is that they are different compared to those in DMSO. This suggests that the complexes **1** and **2** probably lose the weak axial solvent molecule. The transformation is almost instantaneous and, once it happens, there are no further changes observed over time. The behavior of **3** and **4** is similar (**Figure S3**): each series of spectra is different with respect to that recorded in DMSO solution and do not change after 48 h.

Overall, the results can be rationalized postulating that the Mo complexes undergo ligand dissociation in aqueous solution; **1** and **2** lose the weak axial solvent molecule, while for **3** and **4** the breaking of the  $\mu$ -4,4'-bipy bridge occurs. The comparison of the spectra indicates that **1** and **3** on one hand ( $\lambda_{\text{max}} = 380\text{--}381$  nm) and **2** and **4** on the other ( $\lambda_{\text{max}} = 383\text{--}384$  nm) behave similarly; therefore, from these data, it can be argued that **1** and **3** give the mononuclear species  $[\text{Mo}^{\text{VI}}\text{O}_2(\text{L}^1)]$  and **2** and **4** give  $[\text{Mo}^{\text{VI}}\text{O}_2(\text{L}^2)]$ .

ESI-MS spectra of the complexes **1–4** were recorded in a mixture MeOH/H<sub>2</sub>O 90/10 v/v in the positive-ion mode. It was not possible to record the spectra in water alone for the scarce solubility of the metal species. The characteristic pattern of molybdenum, due to <sup>92,94,95,96,97,98,100</sup>Mo isotopes, allows to assign unequivocally the nature of the signals (see **Figure 2** and **Figures S4–S6** of the Supporting Information).

For **1** and **2** the "molecular ion" peaks are observed at *m/z* 452.01 and 467.99, respectively, and are attributed to the adducts  $[\text{MoO}_2(\text{L}^{1-2})] + \text{Na}^+$  (**Table S4–S5** and **Figure S4–S5**), suggesting that the solvent ligand (MeOH for **1** and EtOH for **2**), weakly bound in the axial position, is removed in water according to the reaction (3). No *m/z* signals assignable to  $[\text{MoO}_2(\text{L}^{1-2})(\text{Solv})]$  were observed. Less intense peaks of proton and potassium adducts,  $[\text{MoO}_2(\text{L}^{1-2})] + \text{H}^+$  (at 430.03 and 446.01 *m/z* for **1** and **2**, respectively) and  $[\text{MoO}_2(\text{L}^{1-2})] + \text{K}^+$  (at 467.99 and 483.96 *m/z* for **1** and **2**) were also identified. The comparison between the experimental and calculated isotopic pattern for  $[\text{MoO}_2(\text{L}^{1-2})] + \text{H}^+/\text{Na}^+/\text{K}^+$  ion peaks is shown in **Figures S7** and **S8**.



The complexes **3** and **4** (in MeOH/H<sub>2</sub>O 90/10 v/v) show signals similar to **1** and **2**, respectively (**Tables S4–S5** and **Figures 2** and **S6**). In particular, the peaks of

$[\text{MoO}_2(\text{L}^{1-2})]+\text{H}^+/\text{Na}^+/\text{K}^+$  were revealed plus an intense absorption attributable to  $[\text{4,4'-bipy}]+\text{H}^+$  at  $m/z = 157.08$ , suggesting that in solution **3** and **4** transform to  $[\text{MoO}_2(\text{L}^{1-2})]$  and  $4,4'\text{-bipy}$  (reaction (4)). No peaks attributable to  $[\{\text{MoO}_2(\text{L}^{1-2})\}_2(\mu\text{-4,4'-bipy})]$  in the  $m/z$  range 1000-1100 were found and this indicates that in methanol/water the reaction (4) is completely shifted toward right.

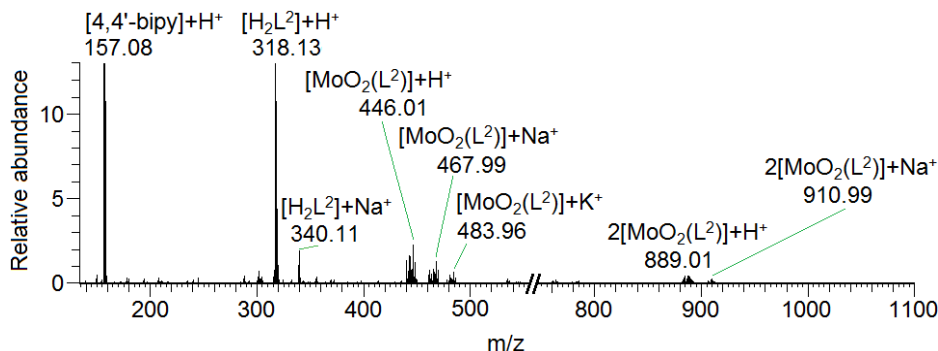


**Figure 2** ESI-MS spectrum recorded in the positive ion mode dissolving the complex **4** in a mixture MeOH/H<sub>2</sub>O 90/10 v/v, 50  $\mu\text{M}$ .



To confirm these insights, the speciation of **1–2** and **3–4** in aqueous media has been also studied by computational methods evaluating the relative stability of the species  $[\text{Mo}^{\text{VI}}\text{O}_2(\text{L}^{1-2})(\text{Solv})]$ ,  $[\{\text{Mo}^{\text{VI}}\text{O}_2(\text{L}^{1-2})\}_2(\mu\text{-4,4'-bipy})]$  and  $[\text{Mo}^{\text{VI}}\text{O}_2(\text{L}^{1-2})]$ , where Solv is MeOH, EtOH and H<sub>2</sub>O. The solvent effect was included in the framework of the SMD model.<sup>69</sup>

Notably, the results indicated that the reactions (3)–(4) are strongly shifted towards right in agreement with ESI-MS measurements. In the hexa-coordinated species  $[\text{MoO}_2(\text{L}^{1-2})(\text{MeOH}/\text{EtOH}/\text{H}_2\text{O})]$ , the monodentate O-ligands leave spontaneously the axial site and cannot be characterized as energy minima. From this finding, it can be argued that

$\Delta G_{\text{aq}}$  is very negative for reaction (3). For the sake of the completeness, the simulations were repeated for **1** in MeOH continuum model; the results indicated that methanol spontaneously leaves the axial site, suggesting that the weak MeOH coordination observed in the X-ray structure could be ascribed to solid state aggregation and stabilization effects in the crystal lattice. Similarly, the dissociation of  $[\{\text{MoO}_2(\text{L}^{1-2})\}_2(\mu\text{-}4,4'\text{-bipy})]$  (reaction (4)) is highly favorable with  $\Delta G_{\text{aq}}$  values of -26.4 and -25.7 kcal mol<sup>-1</sup> for **3** and **4**, respectively. From this analysis, it can be inferred that in aqueous solution the two 5-coordinated species  $[\text{MoO}_2(\text{L}^1)]$  (from **1** and **3**) and  $[\text{MoO}_2(\text{L}^2)]$  (from **2** and **4**) are formed. The optimized structure of  $[\text{Mo}^{\text{VI}}\text{O}_2(\text{L}^{1-2})]$  is shown in **Figure S9**; the electronic and Gibbs energies of the species involved in the equilibria are reported in **Table S6**, while the  $\Delta G$  values in aqueous solution for the reactions (3) and (4) are shown in **Table S7**.

### **Binding to serum bioligands with low molecular mass**

For a potential metallodrug, the study of the interaction with serum bioligands is essential to ascertain its possible biotransformation and the transport of the active species in blood up to the target cells. Obviously, proteins play an important role, in particular HSA (*vide infra*), but the involvement of low molecular mass bioligands (bL) cannot be ignored. Among the serum bL, citrate (citr), lactate (lact), and amino acids, especially histidine (His) may interact with  $[\text{MoO}_2(\text{L}^{1-2})]$  to form ternary  $\text{Mo}^{\text{VI}}\text{O}_2\text{-L}^{1-2}\text{-bL}$  species or the corresponding binary complexes  $\text{Mo}^{\text{VI}}\text{O}_2\text{-bL}$ . The systems were explored by electronic absorption spectroscopy in mixtures H<sub>2</sub>O/MeOH 90/10 v/v, 80/20 v/v and 50/50 v/v varying the pH (5.0 and 7.4), and metal concentration (50 and 10  $\mu\text{M}$ ). The results indicated that no binding occurs (**Figures S10–S11**) and  $[\text{MoO}_2(\text{L}^{1-2})]$  do not form ternary species with the examined bioligands, as also pointed out by DFT methods (*vide infra*).



## HSA binding

### UV-Vis absorption study

After a potential metal-containing drug is administered (orally or intravenously), it enters the bloodstream where the binding with blood carrier proteins such as HSA plays a significant role in assessing its potentiality. The strength of these interactions can determine the overall pharmacokinetic properties of the drugs, such as storage, transport and removal, thereby regulating its efficiency.<sup>82,100</sup>

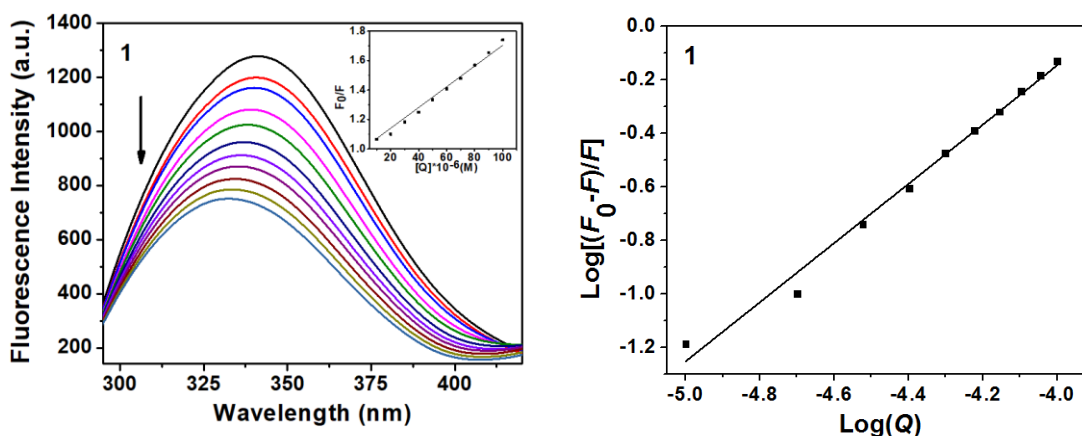


**Figure 3** Fluorescence quenching of HSA (10  $\mu\text{M}$ ) along with successive addition of 10  $\mu\text{M}$  of complex **1** (0–100  $\mu\text{M}$ ) with its Stern-Volmer plot in the inset. Arrow indicates the decrease in fluorescence intensity with respect to an increase in complex concentration. Scatchard plot of **1** is shown in the right panel.

### Fluorescence quenching study

Fluorescence spectroscopy is commonly used to study the binding of potential drugs with serum proteins and to get information on their structure and dynamics in the presence of metal complexes.

Fluorescence emission spectra of HSA, containing one tryptophan moiety, were recorded in the absence and presence of the Mo complexes (quenchers) in 50 mM Tris–HCl buffer (pH 7.4) containing 10% DMF. The intrinsic fluorescence intensity of HSA was significantly quenched upon the gradual addition of increasing concentration of the quencher accompanied with hypsochromic shifts of 10, 14, 11 and 10 nm for the complexes **1**, **2**, **3** and **4**, respectively (**Figures 3** and **S12–S13**). In order to quantitatively estimate the magnitude of interaction between the compounds and HSA, the data were analyzed using the Stern-Volmer equation, which includes a bimolecular quenching rate constant and average life time of the fluorophore as shown in the following equation:<sup>101</sup>

$$\frac{F_0}{F} = 1 + k_q \tau_0 [Q] = 1 + K_{SV} [Q] \quad (5)$$

where  $F$  and  $F_0$  are the fluorescence intensities with and without the quencher, respectively,  $k_q$  the bimolecular quenching rate constant,  $\tau_0$  the average lifetime of fluorophore in the absence of a quencher and  $[Q]$  the concentration of a quencher, *i.e.* the Mo species.  $K_{SV}$  is the Stern–Volmer quenching constant in  $M^{-1}$ . The quenching constants  $K_{SV}$  for the complexes are collected in **Table 1**.

Furthermore, the linear curve of  $F_0/F$  versus  $[Q]$  also suggests a static quenching, *i.e.* formation of fluorophore quencher adducts in the ground state. In protein binding studies, the binding constant (from the intercept) and number of binding sites (from the slope) were obtained using the Scatchard equation, given by:

$$\log \frac{F_0 - F}{F} = \log K_a + n \log [Q] \quad (6)$$

where  $K_a$  and  $n$  are the binding constant and number of binding sites, respectively. It has been demonstrated above that the monomeric and dimeric complexes form one and two equivalents of the penta-coordinated  $[\text{MoO}_2(\text{L}^{1-2})]$  species, respectively, along with the release of the solvent molecule (**1** and **2**) and the co-ligand 4,4'-bipy (**3** and **4**). Hence, for the calculation of the various binding parameters, one mole for monomeric and three moles for the dimeric complexes, considering the contributions to the fluorescence of  $[\text{MoO}_2(\text{L}^{1-2})]$  and 4,4'-bipy, were taken up (**Figures 3** and **S12–S13**). It is noticed that the values of binding constants for monomeric complexes **1** and **2** were close to each other, and similar observation were also made for dimeric complexes **3** and **4**, though experimentally a variance was observed. Overall, the binding constants of the complexes show a reversible binding and release of the complex from HSA. The number of binding sites for all the complexes was found to be  $\sim 1$ .

**Table 1** Parameters obtained from HSA interaction study for complexes **1–4**.

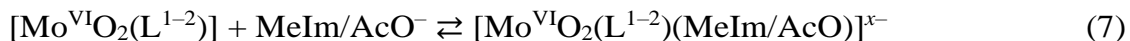
Parameter	Complex			
	<b>1</b>	<b>2</b>	<b>3</b>	<b>4</b>
$K_{SV} (\text{M}^{-1})$	$(7.04 \pm 0.13) \times 10^3$	$(6.80 \pm 0.26) \times 10^3$	$(4.96 \pm 0.10) \times 10^3$	$(3.66 \pm 0.20) \times 10^3$
$k_q (\text{M}^{-1} \text{s}^{-1})$	$(1.13 \pm 0.16) \times 10^{12}$	$(1.10 \pm 0.26) \times 10^{12}$	$(8.02 \pm 0.15) \times 10^{11}$	$(5.92 \pm 0.21) \times 10^{11}$
$K_a (\text{M}^{-1})$	$(1.86 \pm 0.17) \times 10^4$	$(1.37 \pm 0.22) \times 10^4$	$(9.33 \pm 0.19) \times 10^4$	$(2.75 \pm 0.24) \times 10^4$
$n$	$1.10 \pm 0.04$	$0.89 \pm 0.03$	$1.35 \pm 0.02$	$1.24 \pm 0.01$

$K_a$  values, in the range  $10^4$ , highlight a low or moderate interaction of the Mo species with HSA that may lead to a reduction in bioavailability taking into account that only the free

drug can diffuse across cell barriers and reach therapeutic targets.<sup>102</sup> Therefore, HSA may be considered as a good carrier for complexes **1–4**,<sup>103,104</sup> while a higher binding affinity would inhibit the subsequent release of the potential drug, leading to a decrease of *in vivo* anticancer activity.

#### *DFT and docking calculations*

The binding of Mo complexes **1–4** to HSA was also studied by DFT and docking calculations. We demonstrated above that **1–3** and **2–4** undergo transformation in aqueous solution to give the penta-coordinated species [Mo<sup>VI</sup>O<sub>2</sub>(L<sup>1</sup>)] and [Mo<sup>VI</sup>O<sub>2</sub>(L<sup>2</sup>)], which – in the bloodstream – could react with HSA in two ways, through a *coordinative* or a *non-covalent binding* on the protein surface. To evaluate the possibility of formation of a *coordinative binding* through His or Asp/Glu residues, the reaction (7) was considered:



where 1-methylimidazole (MeIm) and acetate (AcO<sup>-</sup>) are models for the binding of His-N or Asp/Glu-COO to molybdenum and *x* is 0 for MeIm and 1 for AcO<sup>-</sup>. The solvent effects were considered through the SMD model for water.<sup>69</sup> The values of Δ*G*<sub>aq</sub> for the formation of [Mo<sup>VI</sup>O<sub>2</sub>(L<sup>1-2</sup>)(MeIm)] and [Mo<sup>VI</sup>O<sub>2</sub>(L<sup>1-2</sup>)(AcO)]<sup>-</sup> are in the range 11.5-12.6 kcal mol<sup>-1</sup>, inducing us to discard the possibility that 6-coordinated species are formed in solution (**Table S7**). These results suggest that the direct coordination of amino acid side-chain of a protein is disfavoured and that HSA interacts with Mo species only in a non-covalent mode. For this reason, only [Mo<sup>VI</sup>O<sub>2</sub>(L<sup>1</sup>)] was used as a model for the classical (non-covalent) blind docking assay.

Docking results for  $[\text{Mo}^{\text{VI}}\text{O}_2(\text{L}^1)]$  with fatted HSA highlight several clusters with similar scoring values ( $F_{\text{max}}$  ranging from 16.2 to 20.0 GoldScore units), indicating the absence of binding specificity.<sup>78</sup> This is in line with the intermediate-low values of the binding constants  $K_a$  (**Table 1**). The best solutions are located at the interfaces of subdomains IIIA/IB (**Figure 4a**) and IIIA/IB (**Figure 4b**); others are found at interface IIIA/IIIB (**Figure 4c**). Each structure is stabilized by at least one hydrogen bond between the aza or  $\text{O}_{\text{furan}}$  functionalities of  $(\text{L}^1)^{2-}$  and/or the oxido ligands with OH group of Tyr or NH groups of Asn, Lys or Arg residues (**Table 2**). It must be highlighted that interfaces IIIA/IB and IIIA/IIIB define an internal pocket in HSA, reported as a common site for ligand interactions including metal species.<sup>105,106</sup> Interestingly, the adducts formed at these sites indicate that the molybdenum species are close to the unique tryptophan (Trp214) of the protein, in agreement with fluorescence quenching experimentally observed.

**Table 2** Blind docking results for the interaction of  $[\text{Mo}^{\text{VI}}\text{O}_2(\text{L}^1)]$  with fatted human serum albumin.

Region	$F_{\text{max}}^{\text{a}}$	$F_{\text{mean}}^{\text{b}}$	Interactions	Pop. <sup>c</sup>	Rank
IIIA/IIIB	20.00	19.12	$\text{NH}_3^+_{,\text{Lys541}} \cdots \text{NN}$ ; $\text{NH}_{2,\text{Arg410}} \cdots \text{MoO}_{\text{ax}}$	4	I
IIA/IB	19.44	17.11	$\text{NH}_{2,\text{Arg222}} \cdots \text{NN}$ ; $\text{NH}_3^+_{,\text{Lys195}} \cdots \text{MoO}_{\text{ax}}$	97	II
IIIA/IB	19.30	18.11	$\text{NH}_{2,\text{Arg196}} \cdots \text{MoO}_{\text{ax/eq}}$ ; $\text{NH}_{2,\text{Gln459}} \cdots \text{MoO}_{\text{eq}}$	13	III
IIIA/IIIB	17.59	16.62	$\text{NH}_3^+_{,\text{Lys541}} \cdots \text{MoO}_{\text{ax}}$ ; $\text{NH}_{2,\text{Arg410}} \cdots \text{MoO}_{\text{eq}}$	21	V
IIIA/IIIB	17.28	16.26	$\text{NH}_3^+_{,\text{Lys541}} \cdots \text{MoO}_{\text{eq}}$ ; $\text{NH}_{,\text{Arg410}} \cdots \text{MoO}_{\text{ax}}$	60	IV
IIIA/IB	16.88	16.14	$\text{NH}_3^+_{,\text{Lys195}} \cdots \text{NN}/\text{O}_{\text{furan}}$ ; $\text{OH}_{\text{Tyr452}} \cdots \text{MoO}_{\text{eq}}$	85	VI
IIA/IB	16.21	15.45	$\text{NH}_{2,\text{Arg257}} \cdots \text{MoO}_{\text{ax}}$	18	VII

<sup>a</sup> *Fitness* value for the most stable pose of each cluster ( $F_{\max}$ ). <sup>b</sup> Mean *Fitness* value of the GoldScore scoring function for each cluster ( $F_{\text{mean}}$ ). <sup>c</sup> Number of solutions in the identified cluster.

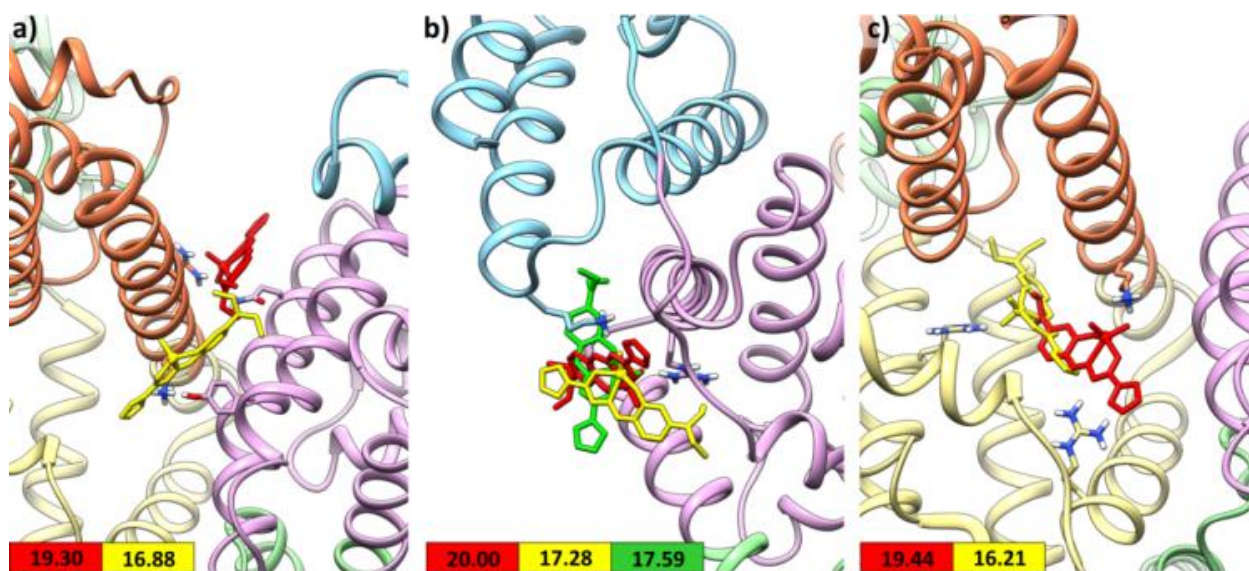


**Figure 4** Best representative solutions of the most stable clusters for the interaction of  $[\text{Mo}^{\text{VI}}\text{O}_2(\text{L}^1)]$  with fatted HSA: a) subdomains IIIA/IB; b) subdomains IIIA/IIIB; c) subdomains IIA/IB, interfaces. Subdomains IIA, IIIA, IB and IIIB, are depicted in yellow, purple, brown and cyan, respectively. Interacting residues are explicitly shown and  $F_{\max}$  values are reported for each cluster with corresponding colors.

#### *Förster resonance energy transfer (FRET)*

In the above section, we mentioned that the molybdenum species are close to the unique tryptophan (Trp214) of HSA. Therefore, fluorescence resonance energy transfer (FRET) was used to estimate the distance between the Trp214 residue and molybdenum species. FRET constitutes a non-destructive spectroscopic method that can provide useful information about the distance of a donor and an acceptor molecule.<sup>85,107</sup> According to Förster's nonradiative energy transfer theory, the efficiency of energy transfer between a

donor and acceptor ( $E$ ), and the average distance between them ( $r_0$ ) can be calculated<sup>85,86</sup> using eq. (8):

$$E = \frac{R_0^6}{R_0^6 + r_0^6} = 1 - \frac{F}{F_0} \quad (8)$$

where  $R_0$  is the distance at 50% transfer efficiency, and  $F$  and  $F_0$  are the observed fluorescence intensities of HSA in the presence and absence of Mo complexes, respectively. The spectral overlap between the normalized donor emission spectrum of HSA and molar extinction coefficient spectrum of the acceptor complexes **1–4** is shown in **Figure S14** and the FRET parameters calculated from eqs. (8) and (1)–(2) are summarized in **Table 3**.

**Table 3** Förster energy transfer parameters for interactions of the complexes **1–4** with HSA.

Complex	$E$	$J$ (nm <sup>4</sup> M <sup>-1</sup> cm <sup>-1</sup> )	$R_0$ (nm)	$r_0$ (nm)
<b>1</b>	0.090	$3.23 \times 10^{14}$	2.90	4.23
<b>2</b>	0.167	$3.88 \times 10^{14}$	2.99	3.88
<b>3</b>	0.163	$5.42 \times 10^{14}$	3.16	4.13
<b>4</b>	0.141	$4.86 \times 10^{14}$	3.11	4.18

The values obtained for  $R_0$  and  $r_0$  are much less than 8 nm which is essential for FRET<sup>108,109</sup> to take place between donor (Trp214) and the specific molybdenum complex (acceptor) bound to HSA (as found from molecular docking study). Furthermore, the obtained  $r_0$  value obeys the relation  $0.5R_0 < r_0 < 1.5R_0$ , which implies that the energy transfer takes place in the interaction with high probability.<sup>108,110,111</sup>

## DNA binding

### *Absorption Titration*

The cytotoxicity of metal complexes is often attributed to their ability to interact with DNA, changing its structure and stability by hydrogen bonding and  $\pi$  stacking between the strands.<sup>112–116</sup>

Electronic absorption spectroscopy is a conventional method used to investigate the interaction of metal complexes with DNA (covalent or non-covalent such as intercalation and electrostatic or groove binding).<sup>117–119</sup> On gradual addition of CT DNA to a solution containing 50 mM Tris–HCl buffer (pH 7.4) containing 10% DMF and the Mo complexes with constant concentration, an appreciable hypochromic shift is observed for the LMCT bands, while absorption bands in the region 275–390 nm show a hyperchromic effect along with a red shift of 8–15 nm (**Figure S15**). The hypochromicity observed in the spectra reveals the presence of charged cations which bind to DNA *via* an electrostatic attraction to the phosphate groups of the DNA backbone, thereby damaging its secondary structure. The hyperchromicity may be also assigned to external contact (electrostatic binding) or to partial uncoiling of the DNA double helical structure, exposing a higher number of its bases. Moreover, an isosbestic spectral change was also observed for **2–4**, which suggests the existence of a chemical equilibrium between the bound and unbound state of the complexes.<sup>117</sup>

The hypochromic shifts in the LMCT absorption bands for each complex were chosen to determine their binding constant ( $K_b$ ) using eq. (9):<sup>120</sup>



$$\frac{[DNA]}{\varepsilon_a - \varepsilon_f} = \frac{[DNA]}{\varepsilon_b - \varepsilon_f} + \frac{1}{K_b(\varepsilon_b - \varepsilon_f)} \quad (9)$$

where,  $\varepsilon_a$ ,  $\varepsilon_f$  and  $\varepsilon_b$  are the apparent extinction coefficients of the complexes in the presence, in absence and to fully bound DNA, respectively,  $[DNA]$  is the concentration of DNA base pairs, and  $K_b$  is the intrinsic binding (equilibrium) constant. The values of  $K_b$ , calculated plotting  $[DNA]/(\varepsilon_a - \varepsilon_f)$  vs.  $[DNA]$ , for the complexes **1–4** were  $2.08 \pm 0.27 \times 10^4$ ,  $1.40 \pm 0.39 \times 10^3$ ,  $2.04 \pm 0.16 \times 10^4$  and  $(2.11 \pm 0.40 \times 10^4)$ , respectively. As described in the *Fluorescence quenching* section, here too, the contribution to the absorbance of two moles of  $[MoO_2(L^{1-2})]$  and one mole of 4,4'-bipy was considered for the calculation of the DNA binding constant. The results indicate a comparable and nearly identical binding affinity for both the monomeric and dimeric complexes. This could be explained with the results of the stability studies in solution and DFT, which suggest that the 4,4'-bipy bridge of the dimeric complexes is broken in aqueous solution to give rise to two monomeric moieties. On the other hand, measurements of the binding of CT DNA with the ligands alone do not reveal any significant interactions.

#### *Competitive DNA binding fluorescence measurements*

The exact mode of binding manifested by the complexes **1–4** with CT DNA was determined with three fluorescent dyes namely EB, DAPI and MG in 50 mM Tris–HCl buffer (pH 7.4) containing 10% DMF through competitive binding experiments, where EB (ethidium bromide) binds to DNA through intercalation, DAPI (4',6-diamidino-2-phenylindole) and MG (methyl green) are minor and major groove binders respectively.<sup>49,121,122</sup> For this study, titration of an increasing complex concentration on EB bound to CT DNA, led to the quenching of the emission intensity of the latter adduct at 597 nm (**Figures S16–S17**). All the complexes exhibited a substantial displacement of the EB bound to CT DNA, which was

in the range of ~50–75%. EB displacement parameters were also calculated through the same approach as described above for the binding interactions with HSA. Hence, the intercalative binding affinity of the complexes were evaluated using the Stern-Volmer equation, giving rise to  $K_{SV}$  values of  $4.41 \pm 0.32 \times 10^3 \text{ M}^{-1}$ ,  $4.35 \pm 0.47 \times 10^3 \text{ M}^{-1}$ ,  $5.26 \pm 0.35 \times 10^3 \text{ M}^{-1}$  and  $4.95 \pm 0.27 \times 10^3 \text{ M}^{-1}$  for complexes **1–4**, respectively. The relevant binding constants ( $K_b$ ) are  $1.85 \pm 0.17 \times 10^3 \text{ M}^{-1}$ ,  $1.58 \pm 0.37 \times 10^3 \text{ M}^{-1}$ ,  $7.33 \pm 0.26 \times 10^3 \text{ M}^{-1}$  and  $2.08 \pm 0.20 \times 10^3 \text{ M}^{-1}$  for complexes **1–4**, respectively, and were derived from Scatchard equation. In this case too, the values are comparable, confirming the dissociation reactions (3) and (4).

In addition, the minor groove binding affinity of **1–4** was assessed by the titration of DAPI bound CT DNA with increasing the complex concentration. There was a decrease in the emission intensity of the DAPI bound to CT DNA at 455 nm, indicating that the complexes could also interact with CT DNA through a minor groove binding (**Figures S18–S19**). Quantitatively, complexes **1–4** were found to be quenched of the emission intensity at 455 nm of ~70, ~66, ~85, ~75% respectively. Therefore, our results clearly demonstrate that **1–4** are able to interact with CT DNA through both intercalation and minor groove binding modes. We also performed similar competitive experiments with MG bound CT DNA; the results suggested that the Mo complexes were not able to quench the emission intensity at 597 nm (data not shown).

#### *Circular Dichroism Study*

Along with the above methods, circular dichroism (CD) spectroscopy was also used to study any conformational modifications taking place in CT DNA upon interaction with the metal complexes. As benchmark, the CD spectra of CT DNA alone reveal a positive band at 275 nm due to base stacking interaction and a negative band at 245 nm due to right handed

helicity.<sup>123,124</sup> Generally, groove binding interactions shows little or no perturbation of the base stacking and helicity bands, while there is a change in the intensity of both bands for intercalation mode.<sup>124,125</sup>

Owing to the interaction with the complexes **1–4**, the CD spectra of the CT DNA showed less change in the positive band at 275 nm, whereas a considerable change was observed in the negative band at 245 nm (**Figure 5**). The results suggested that, along with intercalative mode of binding which is quite evident from the spectra, the Mo complexes could also interact through groove binding and this is in good agreement with the competitive DNA binding results described above.

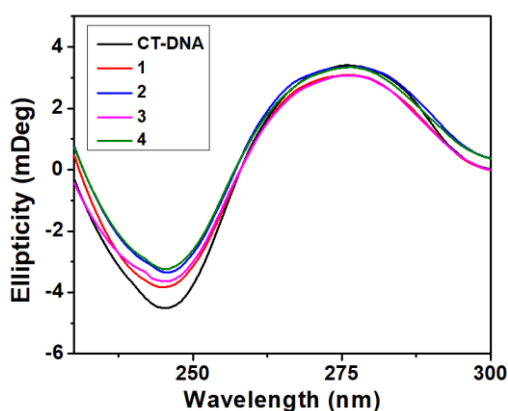


**Figure 5** Circular dichroism spectra of CT DNA (100  $\mu\text{M}$ ) in the presence and absence of **1–4** in 50 mM Tris–HCl buffer (pH 7.4) containing 10% DMF. The path length of the cuvette was 2 mm.

#### *Docking studies*

The binding mechanism of the Mo complexes **1–4** to DNA was also theoretically evaluated. Based on the above mentioned DFT stability studies, the penta-coordinated species  $[\text{Mo}^{\text{VI}}\text{O}_2(\text{L}_1)]$  was used as a representative case in a DNA non-covalent docking assay. As a result, a unique fully populated cluster of solutions with high affinity ( $F_{\text{max}} = 62.6$  and  $F_{\text{mean}} = 60.0$  GoldScore units) was predicted, indicating a clear, high specific minor-groove

binding in which the complex is oriented with the  $\text{MoO}_2^{2+}$  moiety toward the solvent (**Figure 6a**).

The stability of the  $\text{Mo}^{\text{VI}}\text{O}_2(\text{L}_1)\text{-DNA}$  adduct stands on the hydrophobic interactions between DNA bases and the aroylhydrazone ligand  $\text{L}_1$ , as highlighted by the Non-Covalent Interaction (NCI<sup>126</sup>) analysis reported in **Figure 6b** with the green blobs. These results are in accordance with the previously discussed spectroscopic evidence.

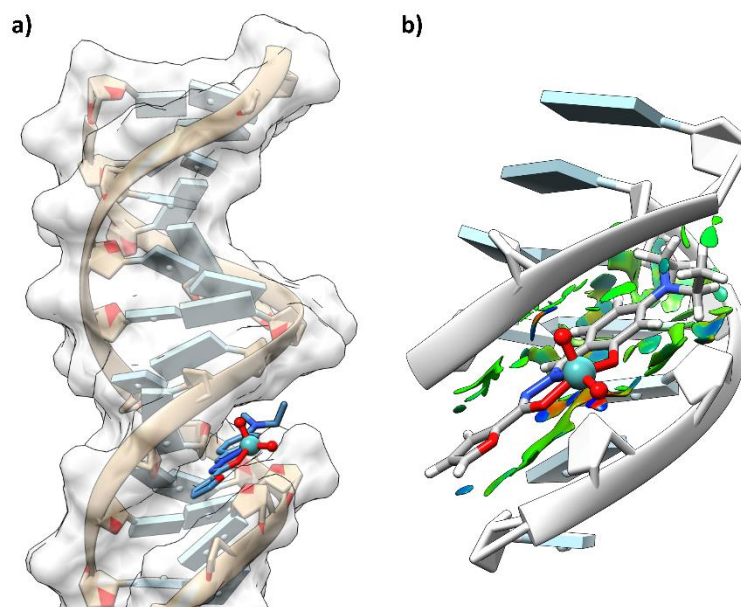


**Figure 6** a) Docking solutions of the  $\text{Mo}^{\text{VI}}\text{O}_2(\text{L}^1)\text{-DNA}$  minor-groove adduct; b) NCI intermolecular analysis. The surfaces are reported in a blue-green-red scale according to values of  $\text{sign}(\lambda_2) \times \rho$ .<sup>127</sup> Blue surfaces indicate strong attractive interactions (such as dipole-dipole or hydrogen bond), red indicates repulsion, while green means van der Waals interaction.

## Cytotoxic activity and mechanism of action

### *Determination of the cytotoxic potential*

In order to determine the cytotoxic effect of the Mo complexes, MTT cell viability assay was carried out.<sup>46,48,49,52</sup> In the present investigation, the complexes – with a different

number of metal centers and substituents in their ligand backbone – were tested for their toxicity on three different cell lines: human cervical cancer (HeLa), human colon cancer (HT-29) and noncancerous mouse embryonic fibroblast (NIH-3T3) cell lines.

**Table 4** IC<sub>50</sub> values of complexes **1–4** for HeLa, HT-29 and NIH-3T3 cell lines.

Complex	IC <sub>50</sub> (μM)		
	HeLa	HT-29	NIH-3T3
<b>1</b>	10.29 ± 2.78	24.14 ± 0.96	41.47 ± 0.84
<b>2</b>	16.42 ± 3.94	25.68 ± 1.32	49.58 ± 0.37
<b>3</b>	9.73 ± 3.90	18.05 ± 1.53	48.60 ± 0.98
<b>4</b>	10.01 ± 2.22	25.04 ± 1.71	51.30 ± 0.52
<b>Cisplatin</b>	12.2	70	4.7

From the results, it can be established that the toxic effects are specific for each compound and are cell type dependent. The aroylhydrazone ligands do not show any significant toxicity compared to the complexes (IC<sub>50</sub> > 100 μM), while the cytotoxicity of 4,4'-bipy is well established in the literature.<sup>128,129</sup> As compared to the other cancer cell line (HT-29), HeLa shows better sensitivity towards all the complexes (**Figure 7**). The IC<sub>50</sub> values indicate that these complexes may act differently on different cell lines ascertaining them to be cell specific. Overall, the IC<sub>50</sub> values for Mo complexes (**Table 4**) were found comparable or also better than cisplatin, a commonly used chemo-therapeutic drug.<sup>130,131,ref</sup> The IC<sub>50</sub> values for all the complexes have been calculated from the cell viability graph and are listed in **Table 4**. The results could be rationalized considering the behavior of **1–4** in aqueous solution. In particular, the dissociation of **3** and **4** complexes results in the release of two moles of penta-coordinated [MoO<sub>2</sub>L<sup>1-2</sup>] species and the cytotoxic 4,4'-bipy molecule.

This mixture of species present in the incubation media may be responsible for comparatively higher cytotoxicity of the dimeric complexes. This finding has been recently demonstrated in the metal systems where the active species could be more than one depending on the conditions; this is particularly evident for vanadium compounds, for which the ligand exchange, redox and chemical changes play a fundamental role to determine the active species in the organism.<sup>17,36,38,132–137</sup> Therefore, similar type of behavior could be postulated for the present systems. This insight further supports the data in the literature that, for metal complexes, the biotransformation under biological media must be taken into account to explain the activity of a potential metal-based drug.

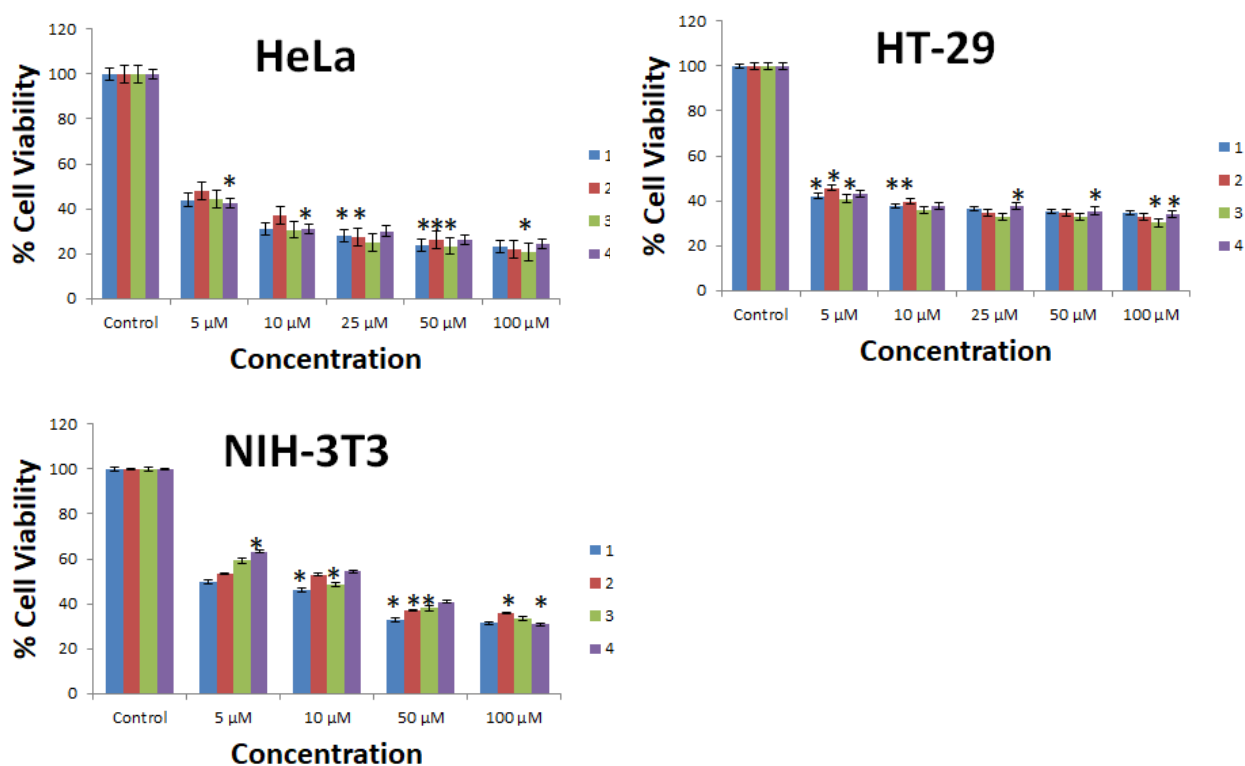


**Figure 7** Cytotoxicity profiles of complexes 1–4 for HeLa, HT-29 and NIH-3T3 cell lines. The cells were subjected to treatment with varying concentrations of the Mo complexes for 48 h and the cell viability was measured using the MTT assay. Data are reported as the mean

± SD for n = 4 and \* represents a statistical significance of  $p < 0.05$  as compared to the control.

So, to further establish the cell specificity of the Mo complexes and – in turn – to study their anticancer properties, **1–4** were evaluated for their cytotoxicity against noncancerous mouse embryonic fibroblast (NIH-3T3) cell line. The results demonstrated that they were significantly less toxic towards the noncancerous than cancerous cells (**Figure 7**). Therefore, it would be safe to claim that these complexes deserve to be further studied as potential anticancer agents in other cell lines in the future.

The present set of complexes has shown superior or similar cytotoxicity when compared to our investigations on other molybdenum(VI) species of aroylhydrazone ligands ( $IC_{50}$  between 4.41 and 162.55  $\mu\text{M}$  for HeLa and  $IC_{50}$  between 20.63 and 177.92  $\mu\text{M}$  for HT-29),<sup>46,97</sup> and salan ( $IC_{50}$  between 10.74 and 275.20  $\mu\text{M}$  for HeLa and  $IC_{50}$  between 2.62 and 221.81  $\mu\text{M}$  for HT-29).<sup>50</sup> They are even better than what was reported for molybdenum(VI) complexes of Schiff base ligands ( $IC_{50}$  between 17 and 58  $\mu\text{M}$  for HeLa<sup>138</sup>) and for molybdenum(V) complexes of neutral bidentate ligands ( $LC_{50}$  35  $\mu\text{M}$  for HeLa from other groups<sup>139</sup>).

#### *Reduction by cellular reductants*

Since complexes **1–4** contain Mo in the oxidation state +VI, their tendency to be reduced to a lower oxidation state has been verified by EPR, ESI-MS and UV-Vis spectroscopy, studying the reaction with cellular reducing agents such as L-ascorbic acid (Asc) and glutathione (GSH), which are present in the cellular environment.

The EPR studies were carried out at physiological pH in mixtures PBS/DMSO 1/1 (v/v) containing the reductants and the Mo complexes in molar ratios ranging from 1/1 to 10/1. In all the cases, the reduction of  $\text{Mo}^{\text{VI}}$  did not take place and it was not possible to reveal any

spectral signals attributable to  $\text{Mo}^{\text{V}}$  which – having a  $4d^1$  electronic configuration– is easily detectable by EPR.<sup>140–142</sup> However, a bielectronic reduction to  $\text{Mo}^{\text{IV}}$  ( $4d^2$ ) could not be detectable by EPR due to the large zero-field splitting and fast relaxation time.<sup>143,144</sup> Therefore, by EPR the reduction to  $\text{Mo}^{\text{V}}$  but not to  $\text{Mo}^{\text{IV}}$  can be excluded.

To get other information on the possible reduction of **1** and **2**, several experiments were carried through the combined application of ESI-MS and UV-Vis with GSH and Asc in mixtures  $\text{H}_2\text{O}/\text{MeOH}$ , at different pH (5.0 and 7.4), metal concentration (5, 10 and 50  $\mu\text{M}$ ) and reductant/Mo ratio (1/1 and 10/1). In the ESI-MS spectra recorded with **1** only the peaks of  $[\text{MoO}_2(\text{L}^1)]$  ( $[\text{MoO}_2(\text{L}^1)]+\text{H}^+/\text{Na}^+/\text{K}^+$  at  $m/z$  430.03, 452.01 and 467.99, respectively) and no signals of other Mo species were detected; moreover, the peaks of uncomplexed GSH ( $[\text{GSH}]+\text{H}^+$  at  $m/z$  308.09) and Asc ( $[\text{Asc}]+\text{H}^+$  and  $[\text{Asc}]+\text{Na}^+$  at  $m/z$  199.02) were observed, while the possible peaks due to the oxidation products, GSSG and L-dehydroascobate (for which the possible adducts with  $\text{H}^+$  and  $\text{Na}^+$  are expected at  $m/z$  613.16 and 635.15, and at 175.02 and 197.01, respectively) were not revealed (**Figure S20**). The UV-Vis spectra with  $[\text{MoO}_2(\text{L}^{1-2})]$  do not show any appreciable variation, so the reduction and/or complexation could be excluded (**Figures 8 and S21**). Moreover, a lower energy UV-Vis absorption peak is expected due to a d–d transition, if  $\text{Mo(VI)}$  would have been reduced to  $\text{Mo(IV)}$  or  $\text{Mo(V)}$ ;<sup>95,99</sup> as this was not the case, this possibility could be further ruled out.

Therefore, the results demonstrate that the studied Mo species are stable and do not have any tendency to be reduced even in the presence of cellular reductants. This finding has as a consequence that Fenton-like reactions could be precluded for complexes **1–4**.



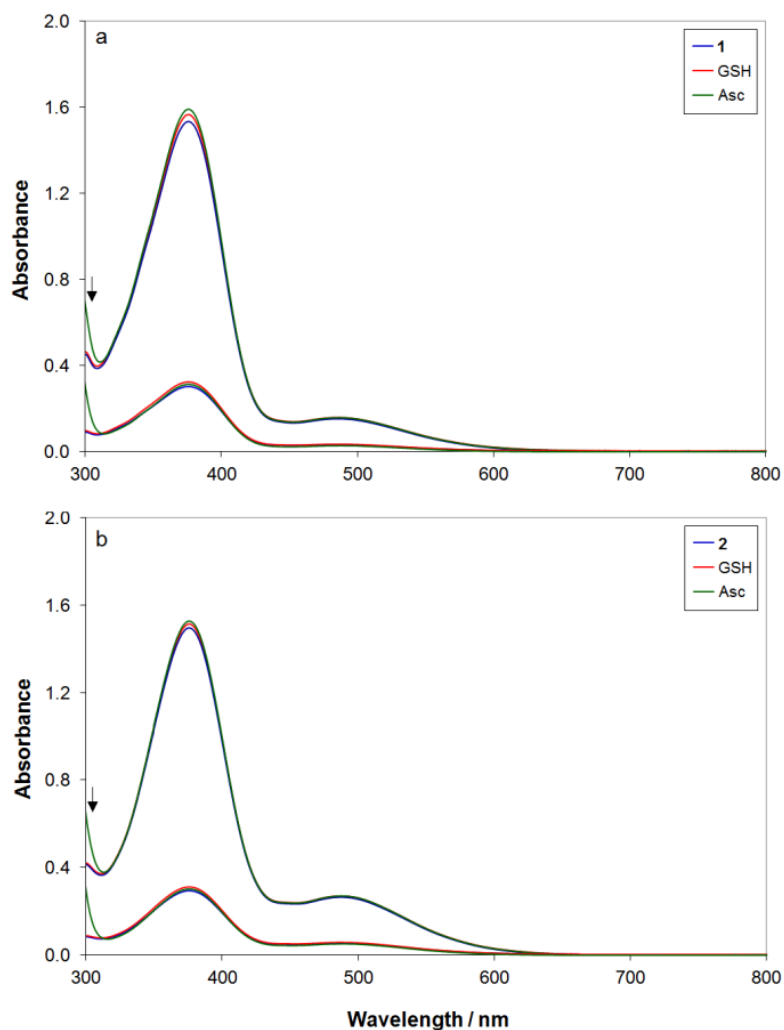


**Figure 8** Electronic absorption spectra recorded on the systems containing  $[\text{MoO}_2(\text{L}^{1-2})]$  (**1**–**2**) and GSH or Asc with molar ratio 1/1, 50 and 10  $\mu\text{M}$ , pH 7.4: a) **1**,  $\text{H}_2\text{O}/\text{MeOH}$  90/10 v/v; b) **2**,  $\text{H}_2\text{O}/\text{MeOH}$  80/20 v/v. With the arrow the absorption of free Asc ligand is shown.

#### *DMPO assay*

The formation of hydroxyl radicals  $\cdot\text{OH}$  was evaluated by DMSO assay according to the procedure established in the literature.<sup>145</sup> Under biological conditions the hydroxyl radicals, taken as representative examples of ROS, can be generated by Fenton-like reactions when both peroxide  $\text{H}_2\text{O}_2$  and a metal species are present in the organism and can cause serious damages to the DNA.<sup>146,147</sup> In the assay, a metal ion or metal complex reacts with  $\text{H}_2\text{O}_2$

hydrogen peroxide, forming  $\cdot\text{OH}$  that is trapped by DMPO to yield the stable radical adduct DMPO–OH, revealed in its turn by EPR spectroscopy with a distinctive four-lines signal with a 1:2:2:1 ratio between the resonances.<sup>148</sup>

The assay was carried out in the systems containing the Mo complexes **1–4** and  $\text{H}_2\text{O}_2$  in the absence or presence of a reducing agent (GSH or ascorbate with a concentration 10 times higher than the metal species). The results show that in both the situations EPR signal was not detected and  $\cdot\text{OH}$  radicals are not produced (**Figure S22**). This confirms the results discussed in the previous section, *i.e.* that  $\text{Mo}^{\text{VI}}$  complexes are not reduced to lower oxidation states which should give the Fenton-like reaction(s)  $\text{Mo}^{\text{V/IV}} + \text{H}_2\text{O}_2 \rightarrow \text{Mo}^{\text{VI/V}} + \text{OH}^- + \cdot\text{OH}$ . In contrast, no Fenton-like process is expected with  $\text{Mo}^{\text{VI}}$ . So, the mechanism of action of **1–4** could not be based on the production of ROS but on the direct interaction with DNA, which was demonstrated by absorption, fluorescence and CD spectroscopy and by docking calculations (*vide supra*).

#### *Nuclear staining*

The mode of cell death (apoptotic or necrotic) induced by the Mo complexes was determined through DAPI staining, which is a DNA binding dye. In line with MTT cell viability results,  $\text{IC}_{50}$  concentration of **1–4** was used in the staining study. Interestingly, it was observed that the complexes cause cell death through apoptotic pathway since the treated cells showed damaged DNA along with disrupted nuclear morphology, nuclear fragmentation and chromatin condensation. In contrast, the nucleus appeared perfectly intact in the control cells with a homogeneous shape (**Figures 9** and **S23**). This confirms that the mode of action of Mo compounds **1–4** must be explained with the interaction with DNA.

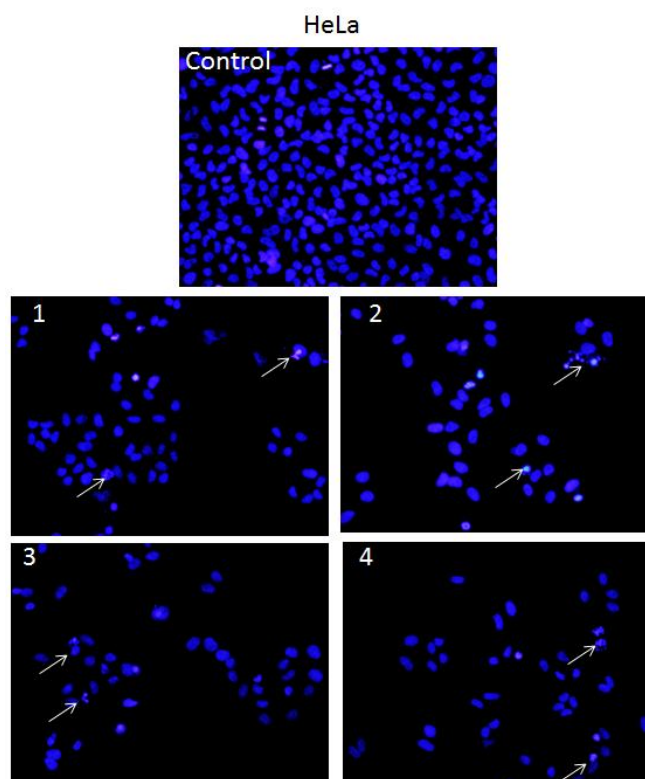


**Figure 9** Changes of HeLa cells observed by fluorescence microscopy upon staining with DAPI following treatment with **1–4** (scale bar corresponds to 20  $\mu\text{m}$ ).

### *Cell Cycle Analysis*

Cell cycle is of paramount importance in cell division and involves a sequential series of events within the cell.<sup>149,150</sup> Generally, in treatments against cancer, cell cycle arrest is linked to induction of cell apoptosis and consequently to cell death.<sup>151</sup> Keeping in view the preliminary screening results, it was found that HeLa cells showed more sensitivity towards the Mo complexes in comparison to HT-29, and therefore HeLa cells were used for further testing the effect of **1–4** on cell cycle progression and cell apoptosis. For this reason, HeLa cells were exposed to different concentrations of the tested compounds for 24 h and analyzed with flow cytometry.<sup>152</sup>

Interestingly, it was observed that the cell population in sub-G0/G1 phase increased from 1.2% (control) to 4.5, 4.8, 5.1 and 5.3%, for complexes **1–4** respectively at 5  $\mu\text{M}$ . Upon increase in concentration to 10 $\mu\text{M}$ , there was further increase in the population in sub-G0/G1 phase to 7.5, 5.5,

5.9 and 7.6%. As shown in **Figure 10**, there was a decrease in the percentage of cells of the G0/G1 phase at both the tested concentrations. The cell populations in the other cell cycle phases (S and G2/M) decreased with respect to the control. The significant increase in population of the sub-G0/G1 reveals that apoptosis was indeed the mechanism by which these complexes induced cell death.<sup>153</sup>

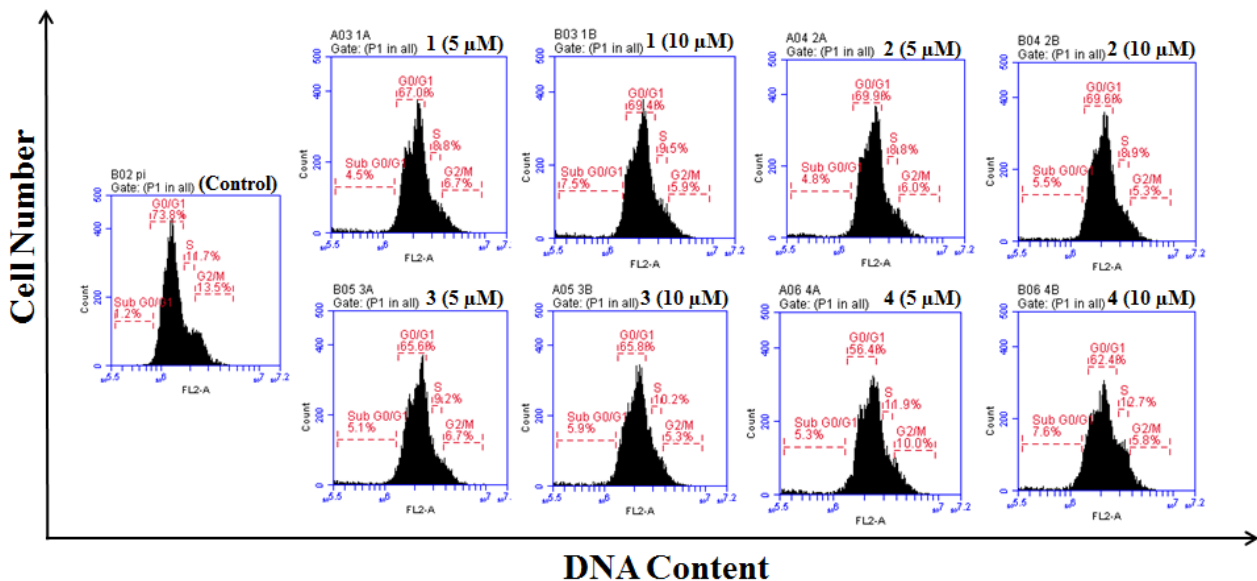


**Figure 10** Percentage of HeLa cells in different phases of cell cycle after 24 h of exposure with complexes 1–4 determined by flow cytometry.

### Cell Apoptosis

Cell death can be attributed to either necrosis or apoptosis. While apoptosis (programmed cell death) is the systematic death of genes controlled by cells that maintain internal stability,<sup>154,155</sup> necrosis (sudden cell death) is usually any sort of injury which results in cell damage. Generally, the competency of an anticancer drug to reduce tumor growth<sup>156</sup> has been linked to its ability to induce apoptosis in cancer cells. Hence, their potential to induce apoptosis in HeLa cells was investigated by flow cytometric analysis after Annexin-V-FITC and propidium iodide (PI) staining. The results presented in **Figure 11** show incubation of HeLa cells with the complexes for 48 h. Quantification of the data indicates that the

percentage of the apoptotic cells (including early and late apoptotic cells) at a concentration of 5  $\mu\text{M}$  was found to be 56.7%, 20.6%, 53.6% and 13.1% for complexes 1–4, respectively. With an increase in the concentrations of Mo complexes, greater populations of cells were found to be in apoptosis. Finally, an 89.6%, 41.3%, 62.1% and 31.5% total proportion of early apoptotic and late apoptotic cells were undergoing apoptosis at a concentration of 10  $\mu\text{M}$ . In the same place, the untreated cells remained 90.3% and 95.0% viable. Altogether, these results clearly indicate that these sets of complexes could kill human cervical cancer (HeLa) cells via apoptosis, which is a hallmark of an anticancer drug. Similar findings have been commonly reported following drug treatment.<sup>157</sup>

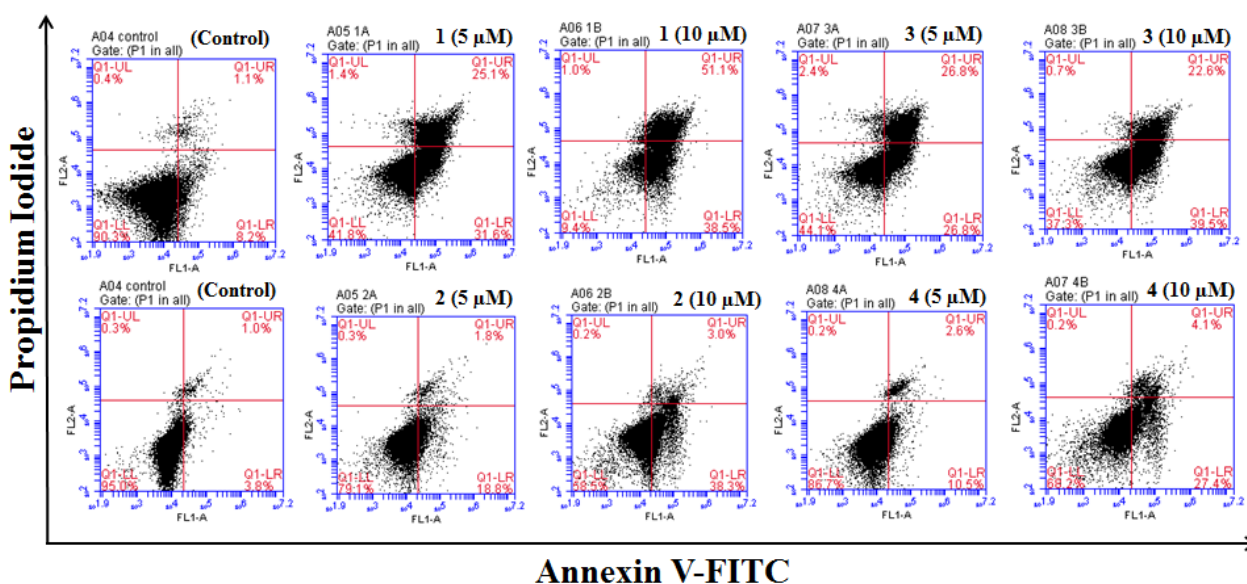


**Figure 11** Induction of apoptosis in HeLa cells treated with 5  $\mu\text{M}$  and 10  $\mu\text{M}$  concentrations of 1–4 for 48 h by flow cytometry using Annexin V/propidium iodide (PI) staining method. The percentage of cell population is indicated as non-apoptotic live cells (lower left), non-apoptotic dead cells (upper left), early apoptotic cells (lower right), and late apoptotic cells (upper right).

## CONCLUSIONS

The results of the present study reveal that the transformation in biological media plays a key role in determining the active species and mode of action of the molybdenum compounds **1–4**. Both mononuclear **1** and **2** and dimeric **3** and **4** Mo complexes undergo chemical changes in solution to give the penta-coordinated species  $[\text{MoO}_2\text{L}^{1-2}]$ . This dissociation process should be taken into account in the analysis of the cytotoxicity for other polynuclear metal-based drugs.  $[\text{MoO}_2\text{L}^{1-2}]$  species are stable and, in the bloodstream, do not bind with low molecular mass bioligands. They only interact non-covalently with HSA before crossing the cellular membrane to enter in the cytosol. The results from the protein binding study suggested that the complexes could interact with HSA through static mode of quenching with reasonably good HSA binding parameters.

In the cytosol, Mo species are redox stable and keep the oxidation state of +VI even in the presence of reducing agents such as ascorbic acid or GSH and reduction of  $\text{Mo}^{\text{VI}}$  to  $\text{Mo}^{\text{V}}$  or  $\text{Mo}^{\text{IV}}$  do not take place. This precludes the Fenton-like reactions and formation of ROS that, indeed, were not detected by EPR spectroscopy. Therefore, the mechanism of cellular toxicity of these complexes could not be related to the production of ROS but to the direct binding with DNA through an intercalative and minor-groove mode, as suggested by *in silico* simulations. The steps that lead from the binding of the Mo complexes to DNA to the cellular apoptosis are not clear at the moment and are currently under investigation in our groups.

Further, the *in vitro* cytotoxicity of **1–4** was assayed against HeLa, HT-29 and NIH-3T3 cell lines. The results unveil the cytotoxicity potential of these complexes as indicated by their ability to induce apoptosis in cancer cell lines. In spite of being fairly cytotoxic in cancer cells, they were less toxic for the noncancerous cells. This could point towards a cancer cell specificity of the complexes. Moreover, among all the tested species, the mixed-ligand

dimeric complexes (**3** and **4**) were comparatively better than their corresponding monomeric complexes (**1** and **2**) towards cytotoxicity. We hypothesize that this effect is due to the presence of a mixture of  $[\text{MoO}_2\text{L}^{1-2}]$  species and 4,4'-bipy after the dissociation of the dimeric **3** and **4** complexes.

The findings of this study should contribute towards the development of molybdenum-based anticancer agents and will pave a path to gain further insights into their mechanism of anticancer activity. Moreover, they confirm that often for a metal-based drug the transformation in biological media can be more important than the molecular nature of the synthesized species in the explanation of the pharmacological action. These chemical changes should be taken into account in the interpretation of the experimental results. In other words, the concept that the administered Mo complex may be only a prodrug, which releases the active species in the serum or cytosol, should be considered in the future in the rational design and development of new potential molybdenum drugs and their drug-delivery strategy.

## ASSOCIATED CONTENT

### Supporting Information

The Supporting Information and crystallographic data in CIF format is available free of charge at DOI: XXXXX.

Crystal data, structure refinement details and selected bond lengths and angles for complexes **1–4** (**Table S1–S3**), identified species in the ESI-MS spectra (**Table S4–S5**), electronic, Gibbs energies of the Mo species and  $\Delta G$  values in aqueous solution for the examined reactions (**Table S6–S7**), molecular structures of **2** and **4** (**Figure S1**), electronic absorption spectrum of **2** (**Figure S2**), time dependent absorption spectra of **1–4** (**Figure S3**), ESI-MS spectra of **1–4** (**Figures S4–S8**), DFT optimized structures of  $[\text{MoO}_2(\text{L}^1)]$  and  $[\text{MoO}_2(\text{L}^2)]$  (**Figure S9**), electronic absorption spectra

recorded on the systems containing  $[\text{MoO}_2(\text{L}^1)]$  and bioligands (**Figures S10–S11**), HSA fluorescence quenching of **2–4** (**Figures S12–S13**), FRET between HSA and **1–4** (**Figure S14**), absorption spectra of **1–4** upon the titration of CT DNA (**Figure S15**), fluorescence quenching of EB and DAPI upon addition of **1–4** (**Figures S16–S19**), ESI-MS and electronic absorption spectra of the systems containing  $[\text{MoO}_2(\text{L}^{1-2})]$  and GSH or Asc (**Figures S20–S21**), EPR spectra of the DMSO assay for **1** and **3** (**Figure S22**), and changes of HT-29 cells observed by fluorescence microscopy upon staining with DAPI of **1–4** (**Figure S23**).

## **AUTHOR INFORMATION**

### **Corresponding Authors**

\*E-mail: [rupamdinda@nitrrkl.ac.in](mailto:rupamdinda@nitrrkl.ac.in) (R. Dinda)

[garribba@uniss.it](mailto:garribba@uniss.it) (E. Garribba)

### **ORCID**

Rupam Dinda: 0000-0001-9452-7791

Eugenio Garribba: 0000-0002-7229-5966

Giuseppe Sciortino: 0000-0001-9657-1788

Daniele Sanna: 0000-0001-9299-0141

Valeria Ugone: 0000-0002-2830-3869

### **Author Contributions**

The manuscript was written through contributions of all authors. All authors have given approval to the final version of the manuscript.

### **Notes**

The authors declare no competing financial interest.

## **ACKNOWLEDGEMENTS**



R. D thanks DBT, Govt. of India [Grant No. 6242-P112/RGCB/ PMD/DBT/RPDA/2015] and CSIR, Govt. of India [Grant No. 01(2963)/18/EMR-II] for funding this research. R. D. also thanks Prof. Werner Kaminsky for help in crystallographic section. G.S., D.S., V.U., and E.G. are thankful to Regione Autonoma della Sardegna (grant RASSR79857) and Fondazione di Sardegna (grant FdSGarribba2017) for financial support. G.S. also thank Spanish MICINN' Juan de la Cierva program, FJC2019-039135-I.

## REFERENCES

- (1) Wheate, N. J.; Walker, S.; Craig, G. E.; Oun, R. The status of platinum anticancer drugs in the clinic and in clinical trials. *Dalton Trans.* **2010**, 39, 8113–8127.
- (2) Levina, A.; Mitra, A.; Lay, P. A. Recent developments in ruthenium anticancer drugs. *Metallomics* **2009**, 1, 458–470.
- (3) Flarakos, J.; Morand, K. L.; Vouros, P. High-throughput solution-based medicinal library screening against human serum albumin. *Anal. Chem.* **2005**, 77, 1345–1353.
- (4) Foye, W. O. *Cancer Chemotherapeutic Agents*, American Chemical Society, Washington, DC, **1995**.
- (5) Arnesano, F.; Losacco, M.; Natile, G., An updated view of cisplatin transport. *Eur. J. Inorg. Chem.* **2013**, 2013, 2701–2711.
- (6) Hoeschele, J. D. In remembrance of Barnett Rosenberg. *Dalton Trans.* **2009**, 10648–10650.
- (7) Reedijk, J. Platinum Anticancer Coordination Compounds: Study of DNA Binding Inspires New Drug Design. *Eur. J. Inorg. Chem.* **2009**, 2009, 1303–1312.
- (8) Raudenska, M.; Balvan, J.; Fojtu, M.; Gumulec, J.; Masarik, M. Unexpected therapeutic effects of cisplatin. *Metallomics* **2019**, 11, 1182–1199.
- (9) Kennard, O. DNA-drug interactions. *Pure Appl. Chem.* **1993**, 65, 1213–1222.
- (10) Hajian, R.; Shams, N.; Mohagheghian, M. Study on the interaction between doxorubicin and deoxyribonucleic acid with the use of methylene blue as a probe. *J. Braz. Chem. Soc.* **2009**, 20, 1399–1405.
- (11) Jones, C. J.; Thornback, J. R. *Medicinal applications of coordination chemistry*. Royal Society of Chemistry: **2007**.
- (12) Dabrowiak, J. C. *Metals in Medicine*; John Wiley & Sons Ltd, Chichester, U.K, **2009**.
- (13) Guo, M.; Sadler, P. J. Competitive binding of the anticancer drug titanocene dichloride to *N,N'*-ethylenebis(*o*-hydroxyphenylglycine) and adenosine triphosphate: a model for Ti<sup>IV</sup> uptake and release by transferrin. *J. Chem. Soc., Dalton Trans.* **2000**, 7–9.
- (14) Olszewski, U.; Hamilton, G. Mechanisms of cytotoxicity of anticancer titanocenes. *Anti-Cancer Agents Med. Chem.* **2010**, 10, 302–311.
- (15) Spreckelmeyer, S.; Orvig, C.; Casini, A. Cellular transport mechanisms of cytotoxic metallodrugs: an overview beyond cisplatin. *Molecules* **2014**, 19, 15584–15610.
- (16) Merlino, A.; Marzo, T.; Messori, L. Protein metalation by anticancer metallodrugs: a joint ESI MS and XRD investigative strategy. *Chem. Eur. J.* **2017**, 23, 6942–6947.

- (17) Levina, A.; Crans, D. C.; Lay, P. A. Speciation of metal drugs, supplements and toxins in media and bodily fluids controls *in vitro* activities. *Coord. Chem. Rev.* **2017**, *352*, 473–498.
- (18) Yeo, C. I.; Ooi, K. K.; Tiekink, E. R. Gold-based medicine: a paradigm shift in anti-cancer therapy? *Molecules* **2018**, *23*, 1410.
- (19) Sigel, A.; Sigel, H.; Freisinger, E.; Sigel, R. K.O. *Metallo-Drugs: Development and Action of Anticancer Agents*. Eds., De Gruyter, **2018**.
- (20) Kiss, T.; Enyedy, É. A.; Jakusch, T.; Dömötör, O. Speciation of metal complexes of medicinal interest: Relationship between solution equilibria and pharmaceutical properties. *Curr. Med. Chem.* **2019**, *26*, 580–606.
- (21) Anthony, E. J.; Bolitho, E. M.; Bridgewater, H. E.; Carter, O. W.; Donnelly, J. M.; Imberti, C.; Lant, E. C.; Lermyte, F.; Needham, R. J.; Palau, M. Metallodrugs are unique: opportunities and challenges of discovery and development. *Chem. Sci.* **2020**, *11*, 12888–12917.
- (22) Merlino, A. Recent advances in protein metalation: structural studies. *Chem. Commun.* **2021**, *57*, 1295–1307.
- (23) Billecke, C.; Finniss, S.; Tahash, L.; Miller, C.; Mikkelsen, T.; Farrell, N. P.; Böglér, O. Polynuclear platinum anticancer drugs are more potent than cisplatin and induce cell cycle arrest in glioma. *Neuro-Oncol.* **2006**, *8*, 215–226.
- (24) M. P. M. Marques, Platinum and Palladium Polyamine Complexes as Anticancer Agents: The Structural Factor. *ISRN Spectroscopy* **2013**, *2013*, 287353.
- (25) Reddy, T. S.; Pooja, D.; Privér, S. H.; Luwor, R. B.; Mirzadeh, N.; Ramesan, S.; Ramakrishna, S.; Karri, S.; Kuncha, M.; Bhargava, S. K. Potent and Selective Cytotoxic and Anti-inflammatory Gold(III) Compounds Containing Cyclometalated Phosphine Sulfide Ligands. *Chem. Eur. J.* **2019**, *25*, 14089–14100.
- (26) Radisavljević, S.; Petrović, B. Gold(III) Complexes: An Overview on Their Kinetics, Interactions With DNA/BSA, Cytotoxic Activity, and Computational Calculations. *Front. Chem.* **2020**, *8*, 379.
- (27) Etcheverry, S. B.; Di Virgilio, A. L.; Nascimento, O. R.; Williams, P. A. Dinuclear copper(II) complexes with valsartan. Synthesis, characterization and cytotoxicity. *J. Inorg. Biochem.* **2012**, *107*, 25–33.
- (28) Fernandes, T. A.; Mendes, F.; Roseiro, A. P.; Santos, I.; Carvalho, M. F. N. Insight into the cytotoxicity of polynuclear Cu(I) camphor complexes. *Polyhedron* **2015**, *87*, 215–219.

- (29) Cindrić, M.; Bjelopetrović, A.; Pavlović, G.; Damjanović, V.; Lovrić, J.; Matković-Čalogović, D.; Vrdoljak, V. Copper(II) complexes with benzhydrazone-related ligands: synthesis, structural studies and cytotoxicity assay. *New J. Chem.* **2017**, *41*, 2425–2435.
- (30) Bhunia, A.; Mistri, S.; Manne, R. K.; Santra, M. K.; Manna, S. C. Synthesis, crystal structure, cytotoxicity study, DNA/protein binding and molecular docking of dinuclear copper (II) complexes. *Inorg. Chim. Acta* **2019**, *491*, 25–33.
- (31) Jeffery, J. C.; Maher, J. P.; Otter, C. A.; Thornton, P.; Ward, M. D. Synthesis of the potentially pentadentate ligand 6,6''-bis (2-hydroxyphenyl)-2,2':6',2''-terpyridine (H<sub>2</sub>L) and the crystal structure and magnetic properties of [Cu(HL)]<sub>2</sub>[PF<sub>6</sub>]<sub>2</sub>·5MeCN. *J. Chem. Soc., Dalton Trans.* **1995**, 819–824.
- (32) Ali, M. A.; Mirza, A. H.; Fereday, R.; Butcher, R. J.; Fuller, J. M.; Drew, S. C.; Gahan, L. R.; Hanson, G. R.; Moubaraki, B.; Murray, K. S. Synthetic, EPR spectroscopic, magnetic and X-ray crystallographic structural studies on copper(II) complexes of the tridentate N<sub>2</sub>S donor ligand formed from 6-methyl-2-formylpyridine and S-methyldithiocarbamate (Hmpsme). *Inorg. Chim. Acta* **2005**, *358*, 3937–3948.
- (33) Koval, I. A.; Sgobba, M.; Huisman, M.; Lüken, M.; Saint-Aman, E.; Gamez, P.; Krebs, B.; Reedijk, J. A remarkable anion effect on the crystal packing of two analogous copper complexes from a thiophene-containing phenol-based ligand. *Inorg. Chim. Acta* **2006**, *359*, 4071–4078.
- (34) Thakurta, S.; Chakraborty, J.; Rosair, G.; Tercero, J.; El Fallah, M. S.; Garribba, E.; Mitra, S. Synthesis of two new linear trinuclear Cu<sup>II</sup> complexes: Mechanism of magnetic coupling through hybrid B3LYP functional and CShM studies. *Inorg. Chem.* **2008**, *47*, 6227–6235.
- (35) Saha, S.; Sasmal, A.; Choudhury, C. R.; Gómez-García, C. J.; Garribba, E.; Mitra, S. A new linear double phenoxide-bridged trinuclear Cu(II) Schiff base complex: Synthesis, crystallographic elucidation, magneto-structural correlation and DFT Study. *Polyhedron* **2014**, *69*, 262–269.
- (36) Banerjee, A.; Dash, S. P.; Mohanty, M.; Sahu, G.; Sciortino, G.; Garribba, E.; Carvalho, M. F. N. N.; Marques, F.; Costa Pessoa, J.; Kaminsky, W.; Brzezinski, K.; Dinda, R. New V<sup>IV</sup>, V<sup>IV</sup>O, V<sup>VO</sup>, and V<sup>VO</sup><sub>2</sub> Systems: Exploring their Interconversion in Solution, Protein Interactions, and Cytotoxicity. *Inorg. Chem.* **2020**, *59*, 14042–14057.
- (37) Sciortino, G.; Sanna, D.; Ugone, V.; Maréchal, J.-D.; Garribba, E. Integrated ESI-MS/EPR/computational characterization of the binding of metal species to proteins: vanadium drug–myoglobin application. *Inorg. Chem. Front.* **2019**, *6*, 1561–1578.

- (38) Yoshikawa, Y.; Sakurai, H.; Crans, D. C.; Micera, G.; Garribba, E. Structural and redox requirements for the action of anti-diabetic vanadium compounds. *Dalton Trans.* **2014**, *43*, 6965–6972.
- (39) Vrdoljak, V.; Đilović, I.; Rubčić, M.; Pavelić, S. K.; Kralj, M.; Matković-Čalogović, D.; Piantanida, I.; Novak, P.; Rožman, A.; Cindrić, M. Synthesis and characterisation of thiosemicarbazonato molybdenum(VI) complexes and their *in vitro* antitumor activity. *Eur. J. Med. Chem.* **2010**, *45*, 38–48.
- (40) Jurowska, A.; Jurowski, K.; Szklarzewicz, J.; Buszewski, B.; Kalenik, T.; Piekoszewski, W. Molybdenum Metallopharmaceuticals Candidate Compounds-The “Renaissance” of Molybdenum Metallodrugs? *Curr. Med. Chem.* **2016**, *23*, 3322–3342.
- (41) Odularu, A. T.; Ajibade, P. A.; Mbese, J. Z. Impact of molybdenum compounds as anticancer agents. *Bioinorg. Chem. Appl.* **2019**, *2019*.
- (42) Majumder, S.; Pasayat, S.; Panda, A. K.; Dash, S. P.; Roy, S.; Biswas, A.; Varma, M. E.; Joshi, B. N.; Garribba, E.; Kausar, C. Monomeric and Dimeric Oxidomolybdenum(V and VI) Complexes, Cytotoxicity, and DNA Interaction Studies: Molybdenum Assisted C=N Bond Cleavage of Salophen Ligands. *Inorg. Chem.* **2017**, *56*, 11190–11210.
- (43) Gretarsdóttir, J. M.; Bobersky, S.; Metzler-Nolte, N.; Suman, S. G. Cytotoxicity studies of water soluble coordination compounds with a  $[\text{Mo}_2\text{O}_2\text{S}_2]^{2+}$  core. *J. Inorg. Biochem.* **2016**, *160*, 166–171.
- (44) Abeysinghe, P. M.; Harding, M. M. Antitumour bis (cyclopentadienyl) metal complexes: titanocene and molybdocene dichloride and derivatives. *Dalton Trans.* **2007**, 3474–3482.
- (45) Honzíček, J.; Vinklárek, J.; Erben, M.; Padělková, Z.; Šebestová, L.; Řezáčová, M. Tetrafluoro-4-pyridyl substituted cyclopentadienyl molybdenum(II) compounds. *J. Organomet. Chem.* **2014**, *749*, 387–393.
- (46) Dinda, R.; Panda, A.; Banerjee, A.; Mohanty, M.; Pasayat, S.; Tiekink, E. R. Investigation of DNA interaction and antiproliferative activity of mixed ligand dioxidomolybdenum(VI) complexes incorporating ONO donor aroylhydrazone ligands. *Polyhedron* **2020**, *183*, 114533.
- (47) Nair, M. L.; Thankaman, D. Synthesis and characterisation of oxomolybdenum(V) and dioxomolybdenum(VI) complexes with Schiff base derived from isonicotinoyl hydrazide. *Indian J. Chem.* **2009**, *48A*, 1212–1218.
- (48) Roy, S.; Mohanty, M.; Pasayat, S.; Majumder, S.; Senthilguru, K.; Banerjee, I.; Reichelt, M.; Reuter, H.; Sinn, E.; Dinda, R. Synthesis, structure and cytotoxicity of a series of

dioxidomolybdenum(VI) complexes featuring Salan ligands. *J. Inorg. Biochem.* **2017**, *172*, 110–121.

(49) Chakraborty, A.; Dash, S. P.; Panda, A. K.; Acharyya, R.; Biswas, A.; Mukhopadhyay, S.; Bhutia, S. K.; Crochet, A.; Patil, Y. P.; Nethaji, M. Synthesis, X-ray structure and *in vitro* cytotoxicity studies of Cu(I/II) complexes of thiosemicarbazone: special emphasis on their interactions with DNA. *Dalton Trans.* **2015**, *44*, 6140–6157.

(50) Pasayat, S.; Dash, S. P.; Roy, S.; Dinda, R.; Dhaka, S.; Maurya, M. R.; Kaminsky, W.; Patil, Y. P.; Nethaji, M. Synthesis, structural studies and catalytic activity of dioxidomolybdenum(VI) complexes with aroylhydrazones of naphthol-derivative. *Polyhedron* **2014**, *67*, 1–10.

(51) Mohanty, M.; Banerjee, A.; Biswal, S.; Horn Jr, A.; Schenk, G.; Brzezinski, K.; Sinn, E.; Reuter, H.; Dinda, R. Polynuclear zinc(II) complexes of thiosemicarbazone: Synthesis, X-ray structure and biological evaluation. *J. Inorg. Biochem.* **2020**, *203*, 110908.

(52) Roy, S.; Mohanty, M.; Miller, R. G.; Patra, S. A.; Lima, S.; Banerjee, A.; Metzler-Nolte, N.; Sinn, E.; Kaminsky, W.; Dinda, R. Probing CO Generation through Metal-Assisted Alcohol Dehydrogenation in Metal-2-(aryloxy) phenol Complexes Using Isotopic Labeling (Metal = Ru, Ir): Synthesis, Characterization, and Cytotoxicity Studies. *Inorg. Chem.* **2020**, *59*, 15526–15540.

(53) Asha, T.; Kurup, M. P. Synthesis, spectroscopy, electrochemistry, crystal structures and *in vitro* cytotoxicity of mononuclear molybdenum (VI) complexes incorporating tridentate ONO donor aroylhydrazone with auxiliary coordination site. *Inorg. Chim. Acta* **2018**, *483*, 44–52.

(54) Asha, T.; Sithambaresan, M.; Kurup, M. P., Dioxidomolybdenum (VI) complexes chelated with N<sup>4</sup>-(3-methoxyphenyl) thiosemicarbazone as molybdenum (IV) precursors in oxygen atom transfer process and oxidation of styrene. *Polyhedron* **2019**, *171*, 530–541.

(55) Kuriakose, D.; Kurup, M. P., Crystal structures and supramolecular architectures of ONO donor hydrazone and solvent exchangeable dioxidomolybdenum (VI) complexes derived from 3, 5-diiodosalicylaldehyde-4-methoxybenzoylhydrazone: Hirshfeld surface analysis and interaction energy calculations. *Polyhedron* **2019**, *170*, 749–761.

(56) Kaymakçioğlu, B. K.; Rollas, S. Synthesis, characterization and evaluation of antituberculosis activity of some hydrazones. *Il Farmaco* **2002**, *57*, 595–599.

(57) Küçükgül, Ş. G.; Rollas, S.; Küçükgül, I.; Kiraz, M. Synthesis and antimycobacterial activity of some coupling products from 4-aminobenzoic acid hydrazones. *Eur. J. Med. Chem.* **1999**, *34*, 1093–1100.

- (58) Chaston, T. B.; Watts, R. N.; Yuan, J.; Richardson, D. R. Potent antitumor activity of novel iron chelators derived from di-2-pyridylketone isonicotinoyl hydrazone involves fenton-derived free radical generation. *Clin. Cancer Res.* **2004**, *10*, 7365–7374.
- (59) Easmon, J.; Pürstinger, G.; Thies, K.-S.; Heinisch, G.; Hofmann, J. Synthesis, structure–activity relationships, and antitumor studies of 2-benzoxazolyl hydrazones derived from alpha-(N)-acyl heteroaromatics. *J. Med. Chem.* **2006**, *49*, 6343–6350.
- (60) Krishnamoorthy, P.; Sathyadevi, P.; Cowley, A. H.; Butorac, R. R.; Dharmaraj, N. Evaluation of DNA binding, DNA cleavage, protein binding and *in vitro* cytotoxic activities of bivalent transition metal hydrazone complexes. *Eur. J. Med. Chem.* **2011**, *46*, 3376–3387.
- (61) Wesselinova, D.; Neykov, M.; Kaloyanov, N.; Toshkova, R.; Dimitrov, G. Antitumour activity of novel 1,10-phenanthroline and 5-amino-1,10-phenanthroline derivatives. *Eur. J. Med. Chem.* **2009**, *44*, 2720–2723.
- (62) Jagadeesan, S.; Balasubramanian, V.; Baumann, P.; Neuburger, M.; Häussinger, D.; Palivan, C. G. Water-soluble Co(III) complexes of substituted phenanthrolines with cell selective anticancer activity. *Inorg. Chem.* **2013**, *52*, 12535–12544.
- (63) Chen, G. J. J.; McDonald, J. W.; Newton, W. E. Synthesis of molybdenum(IV) and molybdenum (V) complexes using oxo abstraction by phosphines. Mechanistic implications. *Inorg. Chem.* **1976**, *15*, 2612–2615.
- (64) Sheldrick, G. M. SHELXT–Integrated space-group and crystal-structure determination. *Acta Cryst.* **2015**, *71*, 3–8.
- (65) Dolomanov, O. V.; Bourhis, L. J.; Gildea, R. J.; Howard, J. A.K.; Puschmann, H. OLEX2: a complete structure solution, refinement and analysis program. *J. Appl. Cryst.* **2009**, *42*, 339–341.
- (66) Frisch, M. J.; Trucks, G. W.; Schlegel, H. B.; Scuseria, G. E.; Robb, M. A.; Cheeseman, J. R.; Scalmani, G.; Barone, V.; Mennucci, B.; Petersson, G. A.; Nakatsuji, H.; Caricato, M.; Li, X.; Hratchian, H. P.; Izmaylov, A. F.; Bloino, J.; Zheng, G.; Sonnenberg, J. L.; Hada, M.; Ehara, M.; Toyota, K.; Fukuda, R.; Hasegawa, J.; Ishida, M.; Nakajima, T.; Honda, Y.; Kitao, O.; Nakai, H.; Vreven, T.; Montgomery, J. A.; Jr., Peralta, J. E.; Ogliaro, F.; Bearpark, M.; Heyd, J. J.; Brothers, E.; Kudin, K. N.; Staroverov, V. N.; Keith, T.; Kobayashi, R.; Normand, J.; Raghavachari, K.; Rendell, A.; Burant, J. C.; Iyengar, S. S.; Tomasi, J.; Cossi, M.; Rega, N.; Millam, J. M.; Klene, M.; Knox, J. E.; Cross, J. B.; Bakken, V.; Adamo, C.; Jaramillo, J.; Gomperts, R.; Stratmann, R. E.; Yazyev, O.; Austin, A. J.; Cammi, R.; Pomelli, C.; Ochterski, J. W.; Martin, R. L.; Morokuma, K.; Zakrzewski, V. G.; Voth, G. A.; Salvador, P.; Dannenberg, J. J.; Dapprich, S.; Daniels, A. D.;

Farkas, Ö.; Foresman, J. B.; Ortiz, J. V.; Cioslowski, J.; Fox, D. J., Eds.; Gaussian 09, revision D.01, Gaussian, Inc., Wallingford, CT, 2010.

(67) Grimme, S.; Antony, J.; Ehrlich, S.; Krieg, H. A consistent and accurate ab initio parametrization of density functional dispersion correction (DFT-D) for the 94 elements H-Pu. *J. Chem. Phys.* **2010**, *132*, 154104.

(68) Ehlers, A. W.; Böhme, M.; Dapprich, S.; Gobbi, A.; Höllwarth, A.; Jonas, V.; Köhler, K. F.; Stegmann, R.; Veldkamp, A.; Frenking, G. A set of f-polarization functions for pseudo-potential basis sets of the transition metals Sc-Cu, Y-Ag and La-Au. *Chem. Phys. Lett.* **1993**, *208*, 111–114.

(69) Marenich, A. V.; Cramer, C. J.; Truhlar, D. G. Universal solvation model based on solute electron density and on a continuum model of the solvent defined by the bulk dielectric constant and atomic surface tensions. *J. Phys. Chem. B* **2009**, *113*, 6378–6396.

(70) Jaque, P.; Marenich, A. V.; Cramer, C. J.; Truhlar, D. G. Computational Electrochemistry: The Aqueous  $\text{Ru}^{3+}|\text{Ru}^{2+}$  Reduction Potential. *J. Phys. Chem. C* **2007**, *111*, 5738–5799.

(71) Weigend, F.; Furche, F.; Ahlrichs, R. Gaussian basis sets of quadruple zeta valence quality for atoms H–Kr. *J. Chem. Phys.* **2003**, *119*, 12753–12762.

(72) Dash, S. P.; Panda, A. K.; Pasayat, S.; Dinda, R.; Biswas, A.; Tiekink, E. R. T.; Patil, Y. P.; Nethaji, M.; Kaminsky, W.; Mukhopadhyay, S. Syntheses and structural investigation of some alkali metal ion-mediated  $\text{LV}^{\text{V}}\text{O}_2^-$  ( $\text{L}^{2-}$  = tridentate ONO ligands) species: DNA binding, photo-induced DNA cleavage and cytotoxic activities. *Dalton Trans.* **2014**, *43*, 10139–10156.

(73) Pace, C. N.; Vajdos, F.; Fee, L.; Grimsley, G.; Gray, T. How to measure and predict the molar absorption coefficient of a protein. *Protein sci.* **1995**, *4*, 2411–2423.

(74) Jones, G.; Willett, P.; Glen, R. C.; Leach, A. R.; Taylor, R. Development and validation of a genetic algorithm for flexible docking. *J. Mol. Biol.* **1997**, *267*, 727–748.

(75) Sciortino, G.; Sanna, D.; Ugone, V.; Micera, G.; Lledós, A.; Maréchal, J.-D.; Garribba, E. Elucidation of binding site and chiral specificity of oxidovanadium drugs with lysozyme through theoretical calculations. *Inorg. Chem.* **2017**, *56*, 12938–12951.

(76) Sciortino, G.; Rodríguez-Guerra Pedregal, J.; Lledós, A.; Garribba, E.; Maréchal, J.-D. Prediction of the interaction of metallic moieties with proteins: An update for protein-ligand docking techniques. *J. Comput. Chem* **2018**, *39*, 42–51.

(77) Sanna, D.; Ugone, V.; Sciortino, G.; Buglyó, P.; Bihari, Z.; Parajdi-Losonczi, P. L.; Garribba, E.  $\text{V}^{\text{IV}}\text{O}$  complexes with antibacterial quinolone ligands and their interaction with serum proteins. *Dalton Trans.* **2018**, *47*, 2164–2182.



- (78) Sciortino, G.; Sanna, D.; Ugone, V.; Lledós, A.; Maréchal, J.-D.; Garribba, E. Decoding surface interaction of V<sup>IV</sup>O metallodrug candidates with lysozyme. *Inorg. Chem.* **2018**, *57*, 4456–4469.
- (79) Sciortino, G.; Sanna, D.; Ugone, V.; Maréchal, J.-D.; Alemany-Chavarria, M.; Garribba, E. Effect of secondary interactions, steric hindrance and electric charge on the interaction of V<sup>IV</sup>O species with proteins. *New J. Chem.* **2019**, *43*, 17647–17660.
- (80) Ugone, V.; Sanna, D.; Sciortino, G.; Maréchal, J.-D.; Garribba, E. Interaction of vanadium(IV) species with Ubiquitin: a combined instrumental and computational approach. *Inorg. Chem.* **2019**, *58*, 8064–8078.
- (81) Sciortino, G.; Garribba, E.; Maréchal, J.-D. Validation and applications of protein–ligand docking approaches improved for metalloligands with multiple vacant sites. *Inorg. Chem.* **2018**, *58*, 294–306.
- (82) Sciortino, G.; Sanna, D.; Lubinu, G.; Maréchal, J.-D.; Garribba, E. Unveiling V<sup>IV</sup>O<sup>2+</sup> Binding Modes to Human Serum Albumins by an Integrated Spectroscopic–Computational Approach. *Chem.–Eur. J.* **2020**, *26*, 11316–11326.
- (83) Bhattacharya, A. A.; Grüne, T.; Curry, S. Crystallographic analysis reveals common modes of binding of medium and long-chain fatty acids to human serum albumin. *J. Mol. Biol.* **2000**, *303*, 721–732.
- (84) Pettersen, E. F.; Goddard, T. D.; Huang, C. C.; Couch, G. S.; Greenblatt, D. M.; Meng, E. C.; Ferrin, T. E. UCSF Chimera—a visualization system for exploratory research and analysis. *J. Comput. Chem.* **2004**, *25*, 1605–1612.
- (85) Hussain, A.; AlAjmi, M. F.; Rehman, M. T.; Amir, S.; Husain, F. M.; Alsalmeh, A.; Siddiqui, M. A.; AlKhedhairi, A. A.; Khan, R. A. Copper(II) complexes as potential anticancer and Nonsteroidal anti-inflammatory agents: *In vitro* and *in vivo* studies. *Sci. Rep.* **2019**, *9*, 5237.
- (86) Parsekar, S. U.; Velankanni, P.; Sridhar, S.; Haldar, P.; Mate, N. A.; Banerjee, A.; Antharjanam, P. S.; Koley, A. P.; Kumar, M. Protein binding studies with human serum albumin, molecular docking and *in vitro* cytotoxicity studies using HeLa cervical carcinoma cells of Cu(II)/Zn(II) complexes containing a carbohydrazone ligand. *Dalton Trans.* **2020**, *49*, 2947–2965.
- (87) Stryer, L.; Haugland, R. P. Energy transfer: a spectroscopic ruler. *Proc. Natl. Acad. Sci. U.S.A.* **1967**, *58*, 719.
- (88) Reichmann, M. E.; Rice, S. A.; Thomas, C. A.; Doty, P. A further examination of the molecular weight and size of desoxypentose nucleic acid. *J. Am. Chem. Soc.* **1954**, *76*, 3047–3053.

- (89) Dash, S. P.; Panda, A. K.; Pasayat, S.; Dinda, R.; Biswas, A.; Tiekink, E. R. T.; Mukhopadhyay, S.; Bhutia, S. K.; Kaminsky, W.; Sinn, E. Oxidovanadium(V) complexes of Aroylhydrazones incorporating heterocycles: Synthesis, characterization and study of DNA binding, photo-induced DNA cleavage and cytotoxic activities. *RSC Adv.* **2015**, *5*, 51852–51867.
- (90) Antonow, D.; Barata, T.; Jenkins, T. C.; Parkinson, G. N.; Howard, P. W.; Thurston, D. E.; Zloh, M. Solution structure of a 2: 1 C2-(2-naphthyl) pyrrolo [2, 1-c][1, 4] benzodiazepine DNA adduct: Molecular basis for unexpectedly high DNA helix stabilization. *Biochemistry* **2008**, *47*, 11818–11829.
- (91) Adão, P.; Majumder, S.; Dash, S. P.; Roy, S.; Kuznetsov, M. L.; Costa Pessoa, J.; Gomes, C. S. B.; Hardikar, M. R.; Tiekink, E. R. T.; Dinda, R. Synthesis, structure, solution behavior, reactivity and biological evaluation of oxidovanadium(IV/V) thiosemicarbazone complexes. *Dalton Trans.* **2018**, *47*, 11358–11374.
- (92) Đukić, M. B.; Jeremić, M. S.; Filipović, I. P.; Klisurić, O. R.; Kojić, V. V.; Jakimov, D. S.; Jelić, R. M.; Onnis, V.; Matović, Z. D. Synthesis, characterization, HSA/DNA interactions and antitumor activity of new  $[\text{Ru}(\eta^6\text{-}p\text{-cymene})\text{Cl}_2(\text{L})]$  complexes. *J. Inorg. Biochem.* **2020**, *213*, 111256.
- (93) Elsayed, S. A.; Badr, H. E.; di Biase, A.; El-Hendawy, A. M. Synthesis, characterization of ruthenium(II), nickel(II), palladium(II), and platinum(II) triphenylphosphine-based complexes bearing an ONS-donor chelating agent: Interaction with biomolecules, antioxidant, *in vitro* cytotoxic, apoptotic activity and cell cycle analysis. *J. Inorg. Biochem.* **2021**, *223*, 111549.
- (94) Enemark, J. H.; Cooney, J. J. A.; Wang, J.-J.; Holm, R. Synthetic analogues and reaction systems relevant to the molybdenum and tungsten oxotransferases. *Chem. Rev.* **2004**, *104*, 1175–1200.
- (95) Dinda, R.; Sengupta, P.; Ghosh, S.; Sheldrick, W. S. Synthesis, structure, and reactivity of a new mononuclear molybdenum(VI) complex resembling the active center of molybdenum oxotransferases. *Eur. J. Inorg. Chem.* **2003**, *2003*, 363–369.
- (96) Dinda, R.; Ghosh, S.; Falvello, L. R.; Tomás, M.; Mak, T. C. Synthesis, structure, and reactivity of some new dipyridyl and diamine-bridged dinuclear oxomolybdenum(VI) complexes. *Polyhedron* **2006**, *25*, 2375–2382.
- (97) Pasayat, S.; Dash, S. P.; Majumder, S.; Dinda, R.; Sinn, E.; Stoeckli-Evans, H.; Mukhopadhyay, S.; Bhutia, S. K.; Mitra, P. Synthesis, structure, characterization and study of antiproliferative activity of dimeric and tetrameric oxidomolybdenum(VI) complexes of *N,N'*-disalicyloylhydrazine. *Polyhedron* **2014**, *80*, 198–205.

- (98) Purohit, S.; Koley, A. P.; Prasad, L. S.; Manoharan, P.; Ghosh, S. Chemistry of molybdenum with hard-soft donor ligands. 2. Molybdenum (VI), -(V), and -(IV) oxo complexes with tridentate Schiff base ligands. *Inorg. Chem.* **1989**, *28*, 3735–3742.
- (99) Dinda, R.; Sengupta, P.; Ghosh, S.; Mayer-Figge, H.; Sheldrick, W. S. A family of mononuclear molybdenum-(VI), and -(IV) oxo complexes with a tridentate (ONO) ligand. *J. Chem. Soc., Dalton Trans.* **2002**, 4434–4439.
- (100) Al-Harhi, S.; Lachowicz, J. I.; Nowakowski, M. E.; Jaremko, M.; Jaremko, Ł. Towards the functional high-resolution coordination chemistry of blood plasma human serum albumin. *J. Inorg. Biochem.* **2019**, *198*, 110716.
- (101) Lin, S.; Wroblewski, S. T.; Hynes, J.; Pitt, S.; Zhang, R.; Fan, Y.; Doweiko, A. M.; Kish, K. F.; Sack, J. S.; Malley, M. F.; Kiefer, S. E.; Newitt, J. A.; McKinnon, M.; Trzaskos, J.; Barrish, J. C.; Dodd, J. H.; Schieven, G. L.; Leftheris, K. Utilization of a nitrogen–sulfur nonbonding interaction in the design of new 2-aminothiazol-5-yl-pyrimidines as p38 $\alpha$  MAP kinase inhibitors. *Bioorg. Med. Chem. Lett.* **2010**, *20*, 5864–5868.
- (102) Dąbrowska, M.; Starek, M.; Skuciński, J. Lipophilicity study of some non-steroidal anti-inflammatory agents and cephalosporin antibiotics: a review. *Talanta* **2011**, *86*, 35–51.
- (103) Mirabelli, C. K.; Johnson, R. K.; Sung, C. M.; Faucette, L.; Muirhead, K.; Crooke, S. T. Evaluation of the *in vivo* antitumor activity and *in vitro* cytotoxic properties of auranofin, a coordinated gold compound, in murine tumor models. *Canc. Res.* **1985**, *45*, 32–39.
- (104) Yilmaz, V. T.; Icsel, C.; Turgut, O. R.; Aygun, M.; Erkisa, M.; Turkdemir, M. H.; Ulukaya, E. Synthesis, structures and anticancer potentials of platinum(II) saccharinate complexes of tertiary phosphines with phenyl and cyclohexyl groups targeting mitochondria and DNA. *Eur. J. Med. Chem.* **2018**, *155*, 609–622.
- (105) Wang, J.; Gou, Y.; Zhang, Z.; Yu, P.; Qi, J.; Qin, Q.; Sun, H.; Wu, X.; Liang, H.; Yang, F. Developing an anticancer copper (II) multitarget pro-drug based on the His146 residue in the IB subdomain of modified human serum albumin. *Mol. Pharm.* **2018**, *15*, 2180–2193.
- (106) Gou, Y.; Qi, J.; Ajayi, J.-P.; Zhang, Y.; Zhou, Z.; Wu, X.; Yang, F.; Liang, H. Developing Anticancer Copper(II) Pro-drugs Based on the Nature of Cancer Cells and the Human Serum Albumin Carrier IIA Subdomain. *Mol. Pharm.* **2015**, *12*, 3597–3609.
- (107) Medintz, I. L.; Hildebrandt, N. *FRET-Förster resonance energy transfer: from theory to applications*; John Wiley & Sons, **2013**.

- (108) Rehman, M. T.; Shamsi, H.; Khan, A. U. Insight into the binding mechanism of imipenem to human serum albumin by spectroscopic and computational approaches. *Mol. Pharm.* **2014**, *11*, 1785–1797.
- (109) Xu, Z.; Liu, Y.; Zhou, S.; Fu, Y.; Li, C. Analysis of the interaction of Dp44mT with human serum albumin and calf thymus DNA using molecular docking and spectroscopic techniques. *Int. J. Mol. Sci.* **2016**, *17*, 1042.
- (110) Ali, M. S.; Amina, M.; Al-Lohedan, H. A.; Al Musayeib, N. M. Elucidation of the interaction of human serum albumin with anti-cancer sipholane triterpenoid from the Red Sea sponge. *Luminescence* **2017**, *32*, 223–230.
- (111) Yue, Y.; Sun, Y.; Dong, Q.; Liu, R.; Yan, X.; Zhang, Y.; Liu, J. Interaction of human serum albumin with novel imidazole derivatives studied by spectroscopy and molecular docking. *Luminescence* **2016**, *31*, 671–681.
- (112) Zhang, C. X.; Lippard, S. J. New metal complexes as potential therapeutics. *Curr. Opin. Chem. Biol.* **2003**, *7*, 481–489.
- (113) Ferguson, L. R.; Denny, W. A. Genotoxicity of non-covalent interactions: DNA intercalators. *Mutat. Res.* **2007**, *623*, 14–23.
- (114) Gkionis, K.; Platts, J. A.; Hill, J. G. Insights into DNA Binding of Ruthenium Arene Complexes: Role of Hydrogen Bonding and  $\pi$  Stacking. *Inorg. Chem.* **2008**, *47*, 3893–3902.
- (115) Aldrich-Wright, J. R.; Vagg, R. S.; Williams, P. A. Design of chiral picen-based metal complexes for molecular recognition of  $\alpha$ -aminoacids and nucleic acids. *Coord. Chem. Rev.* **1997**, *166*, 361–389.
- (116) Jung, Y.; Lippard, S. J. Direct Cellular Responses to Platinum-Induced DNA Damage. *Chem. Rev.* **2007**, *107*, 1387–1407.
- (117) Sathiya Kamatchi, T.; Chitrapriya, N.; Kim, S. K.; Fronczek, F. R.; Natarajan, K. Influence of carboxylic acid functionalities in ruthenium(II) polypyridyl complexes on DNA binding, cytotoxicity and antioxidant activity: Synthesis, structure and *in vitro* anticancer activity. *Eur. J. Med. Chem.* **2013**, *59*, 253–264.
- (118) Sherman, S. E.; Gibson, D.; Wang, A. H. J.; Lippard, S. J. Crystal and molecular structure of *cis*-[Pt(NH<sub>3</sub>)<sub>2</sub>[d(pGpG)]], the principal adduct formed by *cis*-diamminedichloroplatinum(II) with DNA. *J. Am. Chem. Soc.* **1988**, *110*, 7368–7381.
- (119) Strekowski, L.; Wilson, B. Noncovalent interactions with DNA: An overview. *Mutat. Res.* **2007**, *623*, 3–13.

- (120) Ganeshpandian, M.; Loganathan, R.; Suresh, E.; Riyasdeen, A.; Akbarsha, M. A.; Palaniandavar, M. New ruthenium(II) arene complexes of anthracenyl-appended diazacycloalkanes: effect of ligand intercalation and hydrophobicity on DNA and protein binding and cleavage and cytotoxicity. *Dalton Trans.* **2014**, *43*, 1203–1219.
- (121) Satpathi, S.; Sengupta, A.; Hridya, V. M.; Gavvala, K.; Koninti, R. K.; Roy, B.; Hazra, P. A Green Solvent Induced DNA Package. *Sci. Rep.* **2015**, *5*, 9137.
- (122) Prieto, D.; Aparicio, G.; Morande, P. E.; Zolessi, F. R. A fast, low cost, and highly efficient fluorescent DNA labeling method using methyl green. *Histochem. Cell Biol.* **2014**, *142*, 335–345.
- (123) Tjioe, L.; Meiningner, A.; Joshi, T.; Spiccia, L.; Graham, B. Efficient Plasmid DNA Cleavage by Copper(II) Complexes of 1,4,7-Triazacyclononane Ligands Featuring Xylyl-Linked Guanidinium Groups. *Inorg. Chem.* **2011**, *50*, 4327–4339.
- (124) Karidi, K.; Garoufis, A.; Tsipis, A.; Hadjiliadis, N.; den Dulk, H.; Reedijk, J. Synthesis, characterization, *in vitro* antitumor activity, DNA-binding properties and electronic structure (DFT) of the new complex *cis*-(Cl,Cl)[Ru<sup>II</sup>Cl<sub>2</sub>(NO<sup>+</sup>)(terpy)]Cl. *Dalton Trans.* **2005**, 1176–1187.
- (125) Ivanov, V. I.; Minchenkova, L. E.; Schyolkina, A. K.; Poletayev, A. I. Different conformations of double-stranded nucleic acid in solution as revealed by circular dichroism. *Biopolymers* **1973**, *12*, 89–110.
- (126) Contreras-García, J.; Johnson, E. R.; Keinan, S.; Chaudret, R.; Piquemal, J.-P.; Beratan, D. N.; Yang, W. NCIPlot: a program for plotting noncovalent interaction regions. *J. Chem. Theory Comput.* **2011**, *7*, 625–632.
- (127) NCIPlot method bases its estimations computing the reduced gradient of the electron density ( $s$ ) versus the electron density ( $\rho$ ) multiplied by the sign of the second Hessian eigenvalue ( $\lambda_2$ ), i.e.  $\rho \times \text{sign}(\lambda_2)$ . Strong stabilizing interactions (e.g. hydrogen bond type) typically corresponds to values of  $\rho > 0.01$  a.u. and  $\lambda_2 < 0$ . Strong destabilizing interactions (e.g. steric crowding) are associated to values of  $\rho > 0.01$  a.u. and  $\lambda_2 > 0$ . Delocalized weak interactions (e.g. vdW) both density and gradient are small (typically  $\rho < 0.01$  a.u.), and consequently  $\lambda_2$  is also close to 0 ( $\lambda_2 \sim 0$ ).
- (128) Michel-Buono, M.; Buono, J. P.; Serre, G.; Dumont, D.; Bernard, P. *In vitro* cytotoxic effects of 4,4'-bipyridyl on normal human keratinocytes. *Cell Biol. Toxicol.* **1997**, *13*, 193–204
- (129) Li, S.; Crooks, P. A.; Wei, X.; Leon, J. Toxicity of Dipyridyl Compounds and Related Compounds. *Crit. Rev. Toxicol.* **2004**, *34*, 447–460.

- (130) Reytman, L.; Braitbard, O.; Tshuva, E. Y. Highly cytotoxic vanadium(V) complexes of salan ligands; insights on the role of hydrolysis. *Dalton Trans.* **2012**, *41*, 5241–5247 and references therein.
- (131) Stockert, A.; Kinder, D.; Christ, M.; Amend, K.; Aulthouse, A. Improving the Efficacy of Cisplatin in Colon Cancer HT-29 Cells via Combination Therapy with Selenium. *Austin J. Pharmacol. Ther.* **2014**, *2*, 6–12.
- (132) Le, M.; Rathje, O.; Levina, A.; Lay, P. A. High cytotoxicity of vanadium(IV) complexes with 1,10-phenanthroline and related ligands is due to decomposition in cell culture medium. *JBIC, J. Biol. Inorg. Chem.* **2017**, *22*, 663–672.
- (133) Griffin, E.; Levina, A.; Lay, P. A. Vanadium(V) tris-3,5-di-*tert*-butylcatecholato complex: Links between speciation and anti-proliferative activity in human pancreatic cancer cells. *J. Inorg. Biochem.* **2019**, *201*, 110815.
- (134) Sanna, D.; Palomba, J.; Lubinu, G.; Buglyó, P.; Nagy, S.; Perdih, F.; Garribba, E. Role of Ligands in the Uptake and Reduction of V(V) Complexes in Red Blood Cells. *J. Med. Chem.* **2019**, *62*, 654–664.
- (135) Nunes, P.; Correia, I.; Cavaco, I.; Marques, F.; Pinheiro, T.; Avecilla, F.; Costa Pessoa, J. Therapeutic potential of vanadium complexes with 1,10-phenanthroline ligands, *quo vadis?* Fate of complexes in cell media and cancer cells. *J. Inorg. Biochem.* **2021**, *217*, 111350.
- (136) Costa Pessoa, J.; Correia, I. Misinterpretations in Evaluating Interactions of Vanadium Complexes with Proteins and Other Biological Targets. *Inorganics* **2021**, *9*, 17.
- (137) Sanna, D.; Ugone, V.; Micera, G.; Buglyo, P.; Biro, L.; Garribba, E. Speciation in human blood of Metvan, a vanadium based potential anti-tumor drug. *Dalton Trans.* **2017**, *46*, 8950–8967.
- (138) Kazemi, Z.; Rudbari, H. A.; Sahihi, M.; Mirkhani, V.; Moghadam, M.; Tangestaninejad, S.; Mohammadpoor-Baltork, I.; Kajani, A. A. New homochiral and heterochiral Mo(VI) complex from racemic ligand: Synthesis, X-ray structure, diastereomers separation and biological activities. *Polyhedron* **2019**, *170*, 70–85.
- (139) Roy, M.; Biswal, D.; Sarkar, O.; Pramanik, N. R.; Drew, M. G.; Sadhukhan, P.; Kundu, M.; Sil, P. C.; Chakrabarti, S. New mononuclear and binuclear oxomolybdenum(V) complexes containing NN chelator: Syntheses, DFT calculations, interaction with BSA protein and in vitro cytotoxic activity. *J. Inorg. Biochem.* **2019**, *199*, 110755.
- (140) Rajapakshe, A.; Snyder, R. A.; Astashkin, A. V.; Bernardson, P.; Evans, D. J.; Young, C. G.; Evans, D. H.; Enemark, J. H. Insights into the nature of Mo(V) species in solution: Modeling catalytic cycles for molybdenum enzymes. *Inorg. Chim. Acta* **2009**, *362*, 4603–4608.

- (141) Hughes, D. L.; Lowe, D. J.; Mohammed, M. Y.; Pickett, C. J.; Pinhal, N. M. Determination of structural features of electrogenerated *trans*-[MoCl(NMe)(Ph<sub>2</sub>PCH<sub>2</sub>CH<sub>2</sub>PPh<sub>2</sub>)<sub>2</sub>]<sup>2+</sup> by multinuclear electron paramagnetic resonance and electron nuclear double resonance spectroscopy and comparison of interatomic distances with those measured by X-ray analysis of the parent monocation. *J. Chem. Soc., Dalton Trans.* **1990**, 2021–2027.
- (142) Hanson, G.; Berliner, L. *Metals in biology: Applications of high-resolution EPR to metalloenzymes*; Springer, **2010**.
- (143) Drago, R. S. *Physical Methods in Chemistry*, W. B. Saunders Company, Philadelphia, **1977**.
- (144) Mabbs, F. E.; Collison, D. *Electron Paramagnetic Resonance of d Transition Metal Compounds*, Elsevier Science Publishers B.V., Amsterdam, **1992**.
- (145) Buettner, G. R. Spin Trapping: ESR parameters of spin adducts. *Free Radical Biol. Med.* **1987**, 3, 259–303.
- (146) Balasubramanian, B.; Pogozelski, W. K.; Tullius, T. D. DNA strand breaking by the hydroxyl radical is governed by the accessible surface areas of the hydrogen atoms of the DNA backbone. *Proc. Natl. Acad. Sci. U. S. A.* **1998**, 95, 9738–9743.
- (147) Cadet, J.; Delatour, T.; Douki, T.; Gasparutto, D.; Pouget, J.-P.; Ravanat, J.-L.; Sauvaigo, S. Hydroxyl radicals and DNA base damage. *Mutat. Res.* **1999**, 424, 9–21.
- (148) Sanna, D.; Ugone, V.; Fadda, A.; Micera, G.; Garribba, E. Behavior of the potential antitumor V<sup>IV</sup>O complexes formed by flavonoid ligands. 3. Antioxidant properties and radical production capability. *J. Inorg. Biochem.* **2016**, 161, 18–26.
- (149) Icard, P.; Fournel, L.; Wu, Z.; Alifano, M.; Lincet, H. Interconnection between Metabolism and Cell Cycle in Cancer. *Trends Biochem. Sci.* **2019**, 44, 490–501.
- (150) Krall, A. S.; Christofk, H. R. Division enzyme regulates metabolism. *Nature* **2017**, 546, 357–358.
- (151) Peng, Z.; Wang, Y.; Fan, J.; Lin, X.; Liu, C.; Xu, Y.; Ji, W.; Yan, C.; Su, C. Costunolide and dehydrocostuslactone combination treatment inhibit breast cancer by inducing cell cycle arrest and apoptosis through c-Myc/p53 and AKT/14-3-3 pathway. *Sci. Rep.* **2017**, 7, 41254.
- (152) Golla, U.; Adhikary, A.; Mondal, A. K.; Tomar, R. S.; Konar, S. Synthesis, structure, magnetic and biological activity studies of bis-hydrazone derived Cu (ii) and Co (ii) coordination compounds. *Dalton Trans.* **2016**, 45, 11849–11863.
- (153) Haribabu, J.; Srividya, S.; Mahendiran, D.; Gayathri, D.; Venkatramu, V.; Bhuvanesh, N.; Karvembu, R. Synthesis of Palladium (II) Complexes via Michael Addition: Antiproliferative

Effects through ROS-Mediated Mitochondrial Apoptosis and Docking with SARS-CoV-2. *Inorg. Chem.* **2020**, *59*, 17109–17122.

(154) Deswaerte, V.; Nguyen, P.; West, A.; Browning, A. F.; Yu, L.; Ruwanpura, S. M.; Balic, J.; Livis, T.; Girard, C.; Preaudet, A. Inflammasome adaptor ASC suppresses apoptosis of gastric cancer cells by an IL18-mediated inflammation-independent mechanism. *Cancer Res.* **2018**, *78*, 1293–1307.

(155) Cao, Z.; Yang, Q.; Yin, H.; Qi, Q.; Li, H.; Sun, G.; Wang, H.; Liu, W.; Li, J. Peroxynitrite induces apoptosis of mouse cochlear hair cells via a Caspase-independent pathway *in vitro*. *Apoptosis* **2017**, *22*, 1419–1430.

(156) Zhang, T.; Chen, X.; Qu, L.; Wu, J.; Cui, R.; Zhao, Y. Chrysin and its phosphate ester inhibit cell proliferation and induce apoptosis in Hela cells. *Bioorg. Med. Chem.* **2004**, *12*, 6097–6105.

(157) Matos, C. P.; Adiguzel, Z.; Yildizhan, Y.; Cevatemre, B.; Onder, T. B.; Cevik, O.; Nunes, P.; Ferreira, L. P.; Carvalho, M. D.; Campos, D. L. May iron (III) complexes containing phenanthroline derivatives as ligands be prospective anticancer agents? *Eur. J. Med. Chem.* **2019**, *176*, 492–512.



## SYNOPSIS

The transformation of a series of mono- and dimeric molybdenum(VI) complexes in biological media, their interaction with biomolecules and *in vitro* cytotoxicity has been studied. Both the species undergo chemical changes in solution to give the penta-coordinated species  $[\text{MoO}_2(\text{L}^{1-2})]$ . The enhanced biological potential revealed by the dimeric complexes have been attributed to the mixture of  $[\text{MoO}_2(\text{L}^{1-2})]$  species and the cytotoxic 4,4'-bipy molecule.

### FOR TABLE OF CONTENTS ONLY

